HYDROMETEOR PARAMETERS DETERMINED FROM THE RADAR DATA OF THE SAMS RAIN EROSION PROGRAM. AFCRL/SAMS REPORT NO. 2

Vernon G. Plank

Air Force Cambridge Research Laboratories
Hanscom Air Force Base, Massachusetts

4 June 1974

Unclassified
Security Classification

AD/A-005391

DOCUMENT CONTROL DATA - R&D

(Security classification of title, body of abstract and indexing annotation must be entered when the overall report is classified)

1. ORIGINATING ACTIVITY *(Corporate author)* Air Force Cambridge Research Laboratories (LYC) L. G. Hanscom Field Bedford, Massachusetts 01730	2a. REPORT SECURITY CLASSIFICATION Unclassified 2b. GROUP

3. REPORT TITLE

HYDROMETEOR PARAMETERS DETERMINED FROM THE RADAR DATA OF THE SAMS RAIN EROSION PROGRAM - AFCRL/SAMS REPORT NO. 2

4. DESCRIPTIVE NOTES *(Type of report and inclusive dates)*

Scientific. Interim.

5. AUTHOR(S) *(First name, middle initial, last name)*

Vernon G. Plank

6. REPORT DATE 15 May 1974	7a. TOTAL NO. OF PAGES 84	7b. NO. OF REFS 60
8a. CONTRACT OR GRANT NO.	9a. ORIGINATOR'S REPORT NUMBER(S) AFCRL-TR-74-0249	
b. PROJECT, TASK, WORK UNIT NOS. 86200501 c. DOD ELEMENT 63311F d. DOD SUBELEMENT	9b. OTHER REPORT NO(S) *(Any other numbers that may be assigned this report)* ERP No. 477	

10. DISTRIBUTION STATEMENT

Approved for public release; distribution unlimited.

11. SUPPLEMENTARY NOTES	12. SPONSORING MILITARY ACTIVITY Air Force Cambridge Research Laboratories (LYC) L. G. Hanscom Field Bedford, Massachusetts 01730

13. ABSTRACT

The traditional equations relating the radar reflectivity factor and the precipitation rate are reviewed. The hydrometeor and radar parameters involved in the AFCRL/SAMS program at Wallops Island, Virginia, are defined and the methods of measurement and correlation are explained. The hydrometeor regions and transition zones of the Wallops Island storms are discussed and the methods of computing the precipitation rate, the liquid-water-content, and the integral of the liquid-water-content along the trajectories of the SAMS missiles fired into the storms are demonstrated. A case example is presented to illustrate the details of the computational procedures.

The uncertainties of the liquid-water-content values determined from radar measurements are assessed, to a first approximation. Size distribution information is also presented for the different types of hydrometeors, based on theoretical distribution functions.

DD FORM 1 NOV 65 1473

Unclassified
Security Classification

14. KEY WORDS	LINK A		LINK B		LINK C	
	ROLE	WT	ROLE	WT	ROLE	WT
Rain erosion						
Precipitation physics						
Radar meteorology						
Extra tropical storms						
Hydrometeors						
Hydrometeor size distribution						
Hydrometeor measurement						
Uncertainties in storms						
SAMS/ABRES						
Wallops Island, Virginia						

Preface

AFCRL support for the SAMS/ABRES Rain-Erosion Project at Wallops Island, Virginia, during the 1970-73 period covered in this report, was furnished primarily by Air Force and contractor personnel of the Meteorology Laboratory (LY), Directed by Dr. Morton L. Barad. The Laboratory Manager for Weather Erosion Programs was Chankey N. Touart (from June 1973 to present). The Wallops Island Measurement Program was directed by Dr. Robert M. Cunningham. The radar measurement aspects of the program were supervised by Dr. Kenneth R. Hardy.

The AFCRL and contract contributors to the radar measurement program were identified in AFCRL/SAMS Report No. 1. These persons also contributed, directly or indirectly, to the work reported herein.

Personnel associated with the aircraft measurement program supporting SAMS/ABRES at Wallops Island have not been identified previously. The following list of personnel and their work efforts toward the accomplishments of the objectives of the rain-erosion program are acknowledged. Particular thanks are also expressed to Hugh Church of the Sandia Corporation, Albuquerque, N. M., and to Alfred A. Spatola, Lt Col James F. Church, and Elizabeth L. Kintigh of AFCRL for their reviews and criticisms of the manuscript of this report. Their suggestions were most helpful and appreciated.

Name	Organization	Role
LtCol James F. Church	LYC*	Director of Aircraft Measurements
CMSgt Thomas W. K. Hobbs	"	
MSgt Thomas W. Moraski	"	
TSgt James E. Bush	"	
TSgt Stephen Crist	"	
SSgt Dennis E. Karoleski	"	
Sgt David L. Bakke	"	
Sgt Curtis H. Waechtler	"	
Donald Takeuchi	MRI**	
Alfonso Ollivares	"	
Ralph Martin	"	
Larry Boardman	"	

*LYC Convective Cloud Physics Branch, Meteorology Laboratory, AFCRL.
**MRI Meteorology Research Inc., Altadena, California.

The SAMS (Sandia Air Force Materials Study) Program began in 1969 as a jointly funded effort between SAMSO Air Force and Sandia Laboratories. By 1973 all funding was being done by SAMSO. The objective of the SAMS Program is to experimentally test the effects of precipitation and cloud particle (hydrometeor) impacts upon various full scale missile materials by flying high speed vehicles through actual storm and cloud environments. The test vehicle is launched at a relatively low elevation angle (typically 30^{0}) and performs the impact erosion experiment on the ascending portion of its trajectory. The instrumented payload with its test nosetip and heatshield is subsequently recovered from the ocean by means of a parachute and flotation system.

The NASA Wallops Flight Center on the eastern shore of Virginia was selected for the site of these tests because it exhibits a relatively high frequency of occurrence of widespread stratiform storms, has the necessary support facilities, and is readily accessible. Storm environments are measured by instrumented aircraft and ground instruments including special weather radars. Further details of the test set up are contained in the SAMS Program Test Plan, by J.K. Cole, SC-DR-70-850, Sandia Laboratories, Albuquerque, New Mexico, December 1970, while test results are contained in various classified reports from Sandia Laboratories.

Contents

Contents

Illustrations

Illustrations

Tables

Hydrometeor Parameters Determined from the Radar Data of the Sams Rain Erosion Program – AFCRL/Sams Report No. 2

1. INTRODUCTION

The radar equations and measurement techniques of the SAMS rain-erosion program at Wallops Flight Center, Virginia have been described in a previous report by Plank.[1,*] It was noted therein that the end-product radar data for the SAMS missile trajectories consist of measurements of the radar reflectivity factor for water hydrometeors, Z_W, in the lowest storm portion, containing rain, and of the radar reflectivity factor for ice hydrometeors, Z_I, in the upper storm regions, containing snow and ice crystals. It was also mentioned that the values of the reflectivity factor are indeterminant within the melting zone in the storm, since the radar backscattering properties of an ice-water mixture of falling, melting snowflakes are not describable in general quantitative terms, at least, not at present.

The purpose of this report is to explain how the radar values of Z_W and Z_I for the SAMS missile trajectories were used to ascertain the corresponding values of the precipitation rate, P, the precipitation liquid-water-content, M,

(Received for publication 4 June 1974)

1. Plank, V.G. (1974) A summary of the radar equations and measurement techniques used in the SAMS rain erosion program at Wallops Island, Virginia, AFCRL/SAMS Report No. 1, 108 pps, AFCRL-TR-74-0053, Special Reports No. 172, Air Force Cambridge Research Laboratories, Bedford, Mass.

*The name "Wallops Flight Center" was officially designated in May 1974. The facility, prior to this, was called "Wallops Station".

and other related parameters of SAMS interest, such as the size-distribution properties of the hydrometeors.

2. BACKGROUND OF REFLECTIVITY-FACTOR VS PRECIPITATION-RATE RELATIONSHIPS

2.1 Relations for Rain

Wexler,[2] Marshall et al,[3] and Marshall and Palmer[4] were the first to investigate the theoretical-experimental relationships between the back-scattered signals detected by radar and the hydrometeor parameters cited above. Their specific interest involved the possibility of using radar to determine the intensity and distribution of rainfall for hydrological purposes. Wexler, from the data of Laws and Parsons,[5] and Marshall et al, from their own acquired data, ascertained that the radar reflectivity factor for water, Z_W, was related to the precipitation rate, P, approximately as described by the equation

$$Z_W = K P^E , \qquad (1)$$

where P is specified (usually) in mm hr^{-1} and Z_W is given in $mm^6\ m^{-3}$. Wexler found that K had the value 320, with E = 1.44. Marshall et al[3] determined that K = 190 and E = 1.72. Marshall and Palmer[4] presented revised values for the Marshall et al data of K = 220 and E = 1.60. They also reported values, based on other data, of K = 296 and E = 1.47.

Many subsequent investigators have reported particular K and E values for various rainfall situations of experimental observation. These have been reviewed and listed by Sivaramakrishnan,[6] Atlas,[7] Stout and Mueller,[8] Battan,[9] and others.

---

2. Wexler, R. (1947) Radar detection of a frontal storm, 18 June 1946, J. Meteorol. 4:38-44.
3. Marshall, J.S., Langille, R.C., and Palmer, W. McK. (1947) Measurement of rainfall by radar, J. Meteorol. 4(6):186-192.
4. Marshall, J.S., and Palmer, W. McK. (1948) The distribution of raindrops with size, J. Meteorol. 5:165-166.
5. Laws, J.O., and Parsons, D.A. (1943) The relation of raindrop size to intensity, Trans. Amer. Geophys. Union 24(Part II):452-460.
6. Sivaramakrishnan, M.V. (1961) Studies of raindrop size characteristics in different types of tropical rain using a simple raindrop recorder, Indian J. Met. Geophys. 12:189 (473-9, 602, 609, 613).
7. Atlas, D. (1964) Advances in radar meteorology, Adv. Geophys. 10:317 (399, 434, 441, 449, 478, 481).
8. Stout, G.E., and Mueller, E.A. (1968) Survey of relationships between rainfall rate and radar reflectivity in the measurement of precipitation, J. Appl. Meteorol. 7:465 (478-9).
9. Battan, L.J. (1973) Radar Observation of the Atmosphere, the University of Chicago Press, Chicago, Ill.

Battan, for example, lists 69 sets of values for different investigators, geographical locations, seasons, and rainfall type (widespread, orographic, showery). The K values range from 16.6 to 730; the E values from 1.18 to 2.87.

2.2 Relations for Snow

Marshall and Gunn,[10] from the data of Langille and Thain,[11] found that a relationship of the Eq. (1) type could also be applied to the case of snow crystals falling in the atmosphere. Measurements of Z_I were obtained by radar and were correlated with values of P, computed from snowflake samples collected on filter paper during the same time period as the radar measurements. They found that the Marshall and Palmer[4] equation for rain, with K = 220 and E = 1.6, provided a good description of the data. The data were "best fitted" by an equation in which K = 200 and E = 1.6. Imai et al[12] likewise found that a relationship of the Eq. (1) type was descriptive of small snow crystals; their best fit values were K = 500 and E = 1.6. Gunn and Marshall,[13,14] reported that K = 2000, with E = 2.0 for aggregated snow. They additionally mentioned that the snow equation presented earlier by Marshall and Gunn,[10] was probably erroneous, because of problems with the sampling methods used at that time. [However, Carlson and Marshall,[15] with reference to private communication by K. L. S. Gunn, have indicated that the Marshall and Gunn equation is descriptive of single crystal snow.] Austin[16] cited values of K = 1000 and E = 1.6, for heavy snow in the New England area. Her values were intermediate between those of Marshall and Gunn[10] and those of Gunn and Marshall.[13,14]

---

10. Marshall, J. S., and Gunn, K. L. S. (1952) Measurement of snow parameters by radar, J. Meteorol. 9:322.
11. Langille, R. C., and Thain, R. S. (1951) Some quantitative measurements of three centimeter radar echoes from falling snow, Canadian J. Phys. 29:482.
12. Imai, I., Fujiwara, M., Ichimura, I., and Toyama, Y. (1955) Radar reflectivity of falling snow, Pap. in Meteorol. and Geophys. (Japan) 6:130-139.
13. Gunn, K. L. S., and Marshall, J. S. (1956) Size distributions of aggregate snowflakes, Scientific Report NW-20/B, USAF Contract AF19(122)-217, McGill Univ., Montreal, Canada.
14. Gunn, K. L. S., and Marshall, J. S. (1958) The distribution with size of aggregate snowflakes, J. Meteorol. 15:452 (479).
15. Carlson, P. E., and Marshall, J. S. (1972) Measurement of snowfall by radar, J. Appl. Meteorol. 11:494-500.
16. Austin, P. M. (1963) Radar measurements of the distribution of precipitation in New England storms, Proc. 10th Weather Radar Conf., Washington, p. 247 (479, 491-482).

Ohtake and Henmi[17] determined the Z_I vs P relationships for various types of aggregated snowflakes, nine in all, using existing Japanese data concerning size distribution, particle density, and particle fall speeds. Their results, summarized in Table 1, give K values ranging from 330 to 3300 and E values ranging from 1.5 to 2.3.

Table 1. Examples of Z_I Vs P Relationships for Different Types of Aggregated Snowflakes, as Reported by Ohtake and Henmi,[17] Z_I is in $mm^6\ m^{-3}$ and P is in $mm\ hr^{-1}$

Type of Aggregated Snowflakes	Z Vs P Relation
1. Spatial dendrites	$Z_I = 3300\ P^{1.7}$
2. Plane dendrites	$Z_I = 2900\ P^{1.6}$
3. Stellars	$Z_I = 1800\ P^{1.5}$
4. Thick Plates	$Z_I = 1300\ P^{2.3}$
5. Needles	$Z_I = 930\ P^{1.9}$
6. Grauple	$Z_I = 900\ P^{1.6}$
7. Bullets	$Z_I = 430\ P^{1.5}$
8. Plates and Columns	$Z_I = 400\ P^{1.6}$
9. Hail	$Z_I = 330\ P^{1.6}$

Additional information about snow of different types has been presented by authors such as Langleben,[18] Kodaira and Inaba,[19] Litvinov,[20] Bashkirova and Pershina,[21] Kikuchi,[22] Sekhon and Srivastave,[23] and Carlson and Marshall.[15]

17. Ohtake, T., and Henmi, T. (1970) Radar Reflectivity of Aggregated Snowflakes, preprints of papers presented at the 14th Radar Meteorology Conf., Tucson, Arizona, 17-20 November 1970, pp. 209-211.

18. Langleben, M. P. (1954) The terminal velocity of snow aggregates, Quart. J. Meteorol. Soc. 80:174-181.

19. Kodaira, N., and Inaba, M. (1955) Measurement of snowfall intensity by radar, Papers Meteorol. Geophys. (Japan) 6:126-129.

20. Litvinov, I. V. (1956) Determination of the terminal velocity of snowflakes (in Russian), IZV. Akad. Nauk SSSR Ser. Geofiz. No. 7, p. 853 (242).

21. Bashkirova, G., and Pershina, T. (1964) On the mass of snow crystals and their fall velocities, Tr. Gl. Geofiz. Observ. No. 165, 33-100.

22. Kikuchi, K. (1968) On snow crystals of bullet type, J. Meteorol. Soc. Japan 46: 128-132.

23. Sekhon, R. S., and Srivastava, R. C. (1970) Snow size spectra and radar reflectivity, J. Atmos. Sci. 27:299-307.

2.3 Relations for Ice Crystals

Information about the Z_I vs P relationships for single-crystal (non-aggregated) ice crystals has been virtually non-existent in the literature until recently. This is primarily (1) because ice crystals, such as those of SAMS interest that occur in the uppermost portions of storms, seldom exist in the same form aloft as at the ground level, where most previous measurements were made, and (2) because aircraft instruments suitable for measuring the ice crystal types and properties in the storms themselves have not been developed until recently.

Some aircraft measurement data have been acquired since 1970 by the University of Chicago Cloud Physics Laboratory. Optical array spectrometers and formvar replicator instruments were used to determine the size, type, and number concentration of ice crystals in several cirrus-cloud and contrail situations, as described by Knollenberg[24,25,26] and Heymsfield and Knollenberg.[27]

Cunningham, in an AFCRL report of the present series that will be submitted later, has analyzed two sets of ice crystal data supplied to AFCRL by Heymsfield. The data pertain to distribution samples of ice crystals containing columns, bullets, and rosettes. Cunningham's best fit curves (of Eq. (1) type) for the computed Z_I and P values yielded K = 16.1 and E = 1.69 for the first data set, and K = 24.5, with E = 1.39 for the second.

2.4 General Applications to SAMS

Thus far in this background review the Z_W vs P relations for rain and the Z_I vs P relations for snow and ice crystals have been discussed. Typical values and ranges of the constants and exponents of Eq. (1) have been indicated.

Empirical equations of the above form were used in the SAMS rain-erosion program to determine the precipitation rates along the missile trajectories which corresponded to the radar-measured values of Z_W and Z_I. Particular hydrometeor regions were defined for the Wallops storm experiments (rain, large-snow, small-snow, and ice-crystal regions) and particular values of the coefficient, K, and exponent, E, of Eq. (1) were used, as will be described. Other equations of

24. Knollenberg, R.G. (1970) The optical array: An alternative to scattering or extinction for airborne particle size determination, J. Appl. Meteor. 9:86-103.

25. Knollenberg, R.G. (1972) Measurements of the growth of the ice budget in a persisting contrail, J. Atmos. Sci. 29:1367-1374.

26. Knollenberg, R.G. (1973) Cirrus-contrail cloud spectra studies with the Sabreliner, Atmos. Tech., National Center for Atmospheric Research, No. 1, March 1973, pps. 52-55.

27. Heymsfield, A.J., and Knollenberg, R.G. (1972) Properties of cirrus-generating cells, J. Atmos. Sci. 29(7), 1358-1366.

power function form were also used to relate the liquid-water-content values, M, to the precipitation rate, and to interrelate the reflectivity factors, Z_W and Z_I, with the liquid-water content. These latter equations will be presented in a following section.

3. ADDITIONAL BACKGROUND

There are three topics that require perspective discussion at this point before the specifics of the AFCRL analysis program for the SAMS missile shots are described. These topics concern:

(1) the fact that there are three methods of evaluating the radar reflectivity factor that require identification, one defined in terms of radar back-scattering theory, one defined in terms of the actual size-distribution properties of the hydrometeors, and one based on theoretical distribution functions that are presumed to be descriptive of the actual distributions;

(2) the definitions of precipitation rate and liquid water content, together with discussion of how these parameters are measured and interrelated, both at the surface level and at storm levels aloft,

(3) the nature of previous correlation and regression analyses and comments about sampling volumes.

These topics will be discussed in turn in the following sections.

3.1 Different Methods of Evaluating the Radar Reflectivity Factors

As noted in the preceding report (Plank[1]), a weather radar basically measures the summed, backscatter cross-sections of the hydrometeors that are present within the radar pulse volume (or integration volume, if video integration is used). Specifically, the radar measures the volume reflectivity, η, which is the summed backscatter return per unit volume. The radar reflectivity factors, Z_W, for water hydrometeors, and Z_I, for ice hydrometeors, are then determined from the equations (Eqs. (70) and (71) of the cited report),

$$Z_W = \frac{1.08\,\lambda^4\,\eta}{\pi^5} \times 10^{12} \qquad (2)$$

and

$$Z_I = \frac{4.78\,\lambda^4\,\eta}{\pi^5} \times 10^{12}\,, \qquad (3)$$

where λ is the radar wavelength, in cm, η is specified in cm^{-1}, and Z_W and Z_I are in units of $mm^6\ m^{-3}$.

It is important to note that no assumptions about the size distribution properties of the hydrometeors are made when Z_W and Z_I are computed from Eqs. (2) and (3). Such assumptions are unnecessary, since the summed backscatter return from the hydrometeors is being measured directly. The only hydrometeor requirement in the case of these equations is that information be available to differentiate the atmospheric regions containing water hydrometeors from those containing ice hydrometeors; hence to establish which equation, (2) or (3), applies.

For future reference herein, the reflectivity factors computed from Eqs. (2) and (3) will be designated the "reflectivity factors of radar measurement".

The radar reflectivity factors may also be computed from measured or assumed knowledge of the size distribution properties of the hydrometeors. If the knowledge stems from measurements, the reflectivity factor for water hydrometeors is given by

$$Z_{W_M} = \sum_{i=D_{min}}^{i=D_{max}} N(D_i)\, D_i^6 , \tag{4}$$

where $N(D_i)$ is the number of the drops per unit volume (per m^3) of the classified, mid-diameter size, D_i (in mm), and where summation is made from the minimum observed diameter, D_{min}, to the maximum, D_{max}. Analogously, the reflectivity factor for ice hydrometeors is given by

$$Z_{I_M} = \sum_{i=D_{e_{min}}}^{i=D_{e_{max}}} N\left(D_{e_i}\right) D_{e_i}^{\,6} , \tag{5}$$

where D_{e_i} is the "equivalent melted diameter" of the snow or ice crystal particles of the ith equivalent-diameter class. Assumptions must be made in the use of Eq. (5) concerning the "effective density" of the snow aggregates or ice crystals. These are necessary to establish the relations between the physical sizes of the particles and their equivalent melted diameters.

The subscript "M" applied to Z_W and Z_I in Eqs. (4) and (5) signifies that these are particular reflectivity factors computed from direct measurements of size distribution.

Values of the radar reflectivity factors may additionally be obtained by use of theoretical distribution functions which approximate the actual distributions: see, for example, Laws and Parsons,[5] Wexler,[2] Marshall and Palmer,[4] Boucher and

Bartnoff,[28] Gunn and Marshall,[14] Joss et al,[29] and Sekhon and Srivastava.[23] In such case,

$$Z_{W_T} = \int_{D_{min}}^{D_{max}} N\,[f(D)]\, D^6\, dD \tag{6}$$

and

$$Z_{I_T} = \int_{D_{e_{min}}}^{D_{e_{max}}} N\,[f(D_e)]\, D_e^{\,6}\, dD_e\,, \tag{7}$$

where $N\,[f(D)]$ and $N\,[f(D_e)]$ are particular assumed distribution functions and where the subscript "T" on Z_W and Z_I indicate the theoretical nature of the reflectivity factors thus computed.

To illustrate this method of computation, reference is made to the work of Marshall and Palmer[4] concerning rain. They assumed a distribution function of exponential type,

$$N\,[f(D)] = N_D = \alpha\, e^{-\Lambda D}\,, \tag{8}$$

where N_D is the number of drops of diameter D per unit volume per diameter bandwidth. In addition, they assumed that the factor Λ in the exponent was functionally dependent on the precipitation rate, P, in the manner,

$$\Lambda = 41\, P^{-0.21}\ cm^{-1}\,, \tag{9}$$

where the values of the constant and exponent were deduced from observed drop size distributions of rain.

By the substitution of Eq. (9) into (8) into (6), with integration between the diameter limits zero to infinity,*

---

28. Boucher, R. J., and Bartnoff, S. (1955) A Comparison of Theoretically Derived and Observed Drop-Size Distributions in Clouds and Rain, Tufts University, Dept. of Physics, Sci. Rpt No. 4 under Contract AF 19(604)-550, 30 pp.

29. Joss, J., Schram, Karin, Thams, J. C., and Waldvogel, A. (1970) On the Quantitative Determination of Precipitation by Radar, Wissenschaftliche Mitteilung Nr. 63 Forschungsstelle der "Eidgenossischen Kommission zum Studium der Hagelbildung und der Hagelabwehr" am Osservatorio Ticinese della Centrale Meteorologica Svizzera, Locarno-Monti.

*Drops of infinite size do not physically exist, of course, but the equations apply equally well, for practical purposes, to any hydrometeor population in which the largest drops have diameters approximately $\geq 15/\Lambda$ (see Section 7).

$$Z_{W_T} = 3700\ \alpha\ P^{1.47}\ mm^6\ m^{-3}\ . \tag{10}$$

Marshall and Palmer[4] made the further assumption that $\alpha = 0.08$, again supported by data which yielded the equation

$$Z_{W_T} = 296\ P^{1.47}\ mm^6\ m^{-3}\ , \tag{11}$$

which was referenced earlier in the present report.

The Marshall and Palmer method indicated above, involving the use of a distribution function of exponential type, has become a more or less standard method for determining the Z_{W_T} vs P relationships for rain, also the Z_{I_T} vs P relationships for snow and ice crystals (see Gunn and Marshall,[14] Sekhon and Srivastava,[23] and Carlson and Marshall[15]).

Various efforts have been made to truncate the distribution function at diameter limits other than zero and infinity, as by Sekhon and Srivastava,[23,30] but this rapidly leads to mathematical complexity and requirements for additional assumptions.

It can be seen that the distribution-function method requires observational data to provide realistic estimates of the constant α, and of the coefficient and exponent of the Eq. (9) expression (the general expression) for Λ.

3.2 The Hydrometeor Parameters

We turn now to a more detailed consideration of two of the hydrometeor parameters of SAMS interest, the precipitation rate, P, and the liquid-water-content, M.

The precipitation rate is a volume flux parameter that tells the volume of liquid water (in the form of drops or ice particles) that falls across a horizontal surface per unit surface area, per unit time. Thus P has the dimensions LT^{-1}, and it is conventional to employ the particular units $mm\ hr^{-1}$.

The precipitation liquid-water-content is a density parameter that specifies the mass amount of liquid water (of precipitable size) that exists within a unit atmospheric volume.* The dimensions of M are Mass $\times\ L^{-3}$, and the particular units $gm\ m^{-3}$ are customarily utilized.

---

30. Sekhon, R.S., and Srivastava, R.C. (1971) Doppler radar observations of drop size distributions in a thunderstorm, J. Atmos. Sci. 28:983-994.

*A distinction is made between the liquid-water-content of precipitation-size hydrometeors, generally larger than about 80 microns diameter (or equivalent melted diameter), which can be detected by the SAMS radars, and the liquid-water-content of cloud-size hydrometeors of smaller diameter, which cannot be detected by the radars and must be measured by aircraft instruments.

The precipitation rate and liquid-water content may be related, if the fall velocity of the hydrometeors can be specified as a function of their size. Such specification may be made on a size-class by size-class basis, if actual fall velocity data are utilized, or it may be accomplished on the basis of an equation relation that describes the approximate variation of fall velocity with diameter (equivalent diameter in the case of snow or ice crystals). One commonly used relation that pertains to particular, restricted size ranges, seen in the works of Spilhaus,[31] Gunn and Kinzer,[32] and Langleben,[18] for example, is

$$V = a D^b , \tag{12}$$

for water hydrometeors, or

$$V = a D_e^b , \tag{13}$$

for ice hydrometeors, where V is the fall velocity, usually in cm sec^{-1}, and D and D_e are the diameter and equivalent-melted-diameter, respectively.

At the ground surface, it is usually the precipitation rate that is measured directly (by rain gauges, disdrometers, or other means) and the liquid-water-content is derived therefrom. Above the ground surface, on the other hand, in storm regions where aircraft measurements or indirect probing methods are required, it is usually the liquid-water-content that is measured directly and the precipitation rate is derived.

3.2.1 MEASUREMENTS AND DERIVATIONS AT THE GROUND LEVEL

For example, for rain at the ground level when measurement knowledge exists concerning the size-distribution flux of the raindrops, [as acquired by disdrometers, for instance (see Plank[1] for description)] the precipitation rate is given by

$$P = \frac{6\pi}{A_s \Delta t} \sum_{i=D_{min}}^{i=D_{max}} N_f(D_i)\, D_i^3 \text{ mm hr}^{-1} , \tag{14}$$

where $N_f(D_i)$ is the number of drops of the classified diameter size D_i, in mm, that fall across a horizontal sampling area A_s, in cm^2, in a time interval Δt in seconds.

---

31. Spilhaus, A. F. (1948) Raindrop size, shape, and falling speed, J. Meteorol. 5:108-110.

32. Gunn, R., and Kinzer, G. D. (1949) The terminal velocity of fall for water droplets in stagnant air, J. Meteorol. 6:243 (565, 594, 596-7).

The liquid water content of this rain may be determined from information about the fall velocity of the drops (from actual data or equation relations, as mentioned earlier).

If we assume that Eq. (12) describes the fall velocity of the drops, the liquid water content is determined as follows:

The water mass content of any given size-class of the drops is

$$\text{Mass}_{D_i} = \frac{\pi \times 10^{-3} \rho N_f(D_i) D_i^3}{6} \text{ gm}, \tag{15}$$

where ρ is the density of water in gm cm^{-3}, and D_i is measured in mm.

The atmospheric volume (average volume) that contained these drops just prior to their gravitational fall onto the collector is approximately,

$$\text{Vol}_{D_i} = V_{D_i} A_s \Delta t, \tag{16}$$

where V_{D_i} is the fall velocity of the drops. This fall velocity, from Eq. (12), is

$$V_{D_i} = aD_i^b. \tag{17}$$

The liquid water content of the drops of this size class is, by definition, the water mass per unit atmospheric volume. Hence, from Eqs. (15) and (16), also replacing V_{D_i} in Eq. (16) by the Eq. (17) expression,

$$M_{D_i} = \frac{\text{Mass}_{D_i}}{\text{Vol}_{D_i}} = \frac{\pi \times 10^3 \rho N_f(D_i) D_i^{3-b}}{6 a A_s \Delta t} \text{ gm m}^{-3}, \tag{18}$$

where M_{D_i} is given in the conventional units of gm m^{-3} (for A_s specified in cm^2, with Δt in seconds).

The <u>total</u> liquid water content of the distribution of all drop diameters is then given simply by

$$M = \frac{\pi \times 10^3 \rho}{6 a A_s \Delta t} \sum_{i=D_{min}}^{i=D_{max}} N_f(D_i) D_i^{3-b}. \tag{19}$$

The precipitation rate at the surface level may, of course, also be measured <u>without</u> detailed knowledge of the size distribution of the raindrops. Tipping bucket or weighing-type gauges can be used to acquire such information.

For P values obtained directly in this way, it has been customary, in the SAMS work at AFCRL, to assume that the precipitation liquid-water-content is related to P as,

$$M = k P^{\epsilon} , \tag{20}$$

where k and ϵ have differing values dependent on rainfall type. The particular values used will be cited later. Equations of this form, relating M and P, have been described by Marshall and Palmer,[4] Gunn and Marshall,[14] and others.

Although it is possible to measure the precipitation rate at the surface level in snow using rain gauges that heat and melt the frozen particles as they fall into the collector, such instruments were not used at Wallops Island. All of the missile firings thus far were made into storms having rain at the surface level.

3.2.2 MEASUREMENTS AND DERIVATIONS ALOFT

At storm levels above the surface level, aircraft, or other, measurements of hydrometeors usually consist of volumetric samples that provide information about (1) the types, sizes, and numbers of the drops or particles, or (2) the bulk or integrated properties of the hydrometeors, such as their liquid water content.

If size distribution measurements are obtained from aircraft by the use of spectrometer, formvar replicator, or foil-sampling devices, for example, the liquid water content of the distribution is given by,

$$M = \frac{\pi \times 10^{-3} \rho}{6 V_s} \sum_{i=D_{min}}^{i=D_{max}} N_s(D_i) D_i^3 , \tag{21}$$

where $N_s(D_i)$ is the number of the drops of the classified diameter size D_i (or D_{e_i}, in the case of ice hydrometeors) in the sampling volume, V_s, which latter is specified in m^3.

The precipitation rate may be computed from these aircraft, size-distribution measurements by utilizing the fall-velocity data or relations cited earlier and by making the assumption that no updraft or downdraft motions exist in the storm at the altitude of interest. If, for example, we use Eq. (12) to specify the fall velocities of the hydrometeors, the precipitation rate, following the same reasoning steps described in Section 3.2.1, except in reverse, is

$$P = \frac{6 \pi a \times 10^{-6}}{V_s} \sum_{i=D_{min}}^{i=D_{max}} N_s(D_i) D_i^{3+b} \text{ mm hr}^{-1} . \tag{22}$$

When the liquid-water-content is measured directly by the aircraft, as by means of Australian* or total liquid water content meters, or certain spectrometer devices, the corresponding precipitation rate is inferred from the inverted form of Eq. (20), that is

$$P = \left(\frac{M}{k}\right)^{1/\epsilon} , \tag{23}$$

where, as previously mentioned, k and ϵ have particular values dependent on the rain, snow, or ice crystal types detected by the aircraft. The assumption of a static atmosphere, devoid of updraft-downdraft motions, is also implicit in this equation, as with Eq. (22).

3.3 Previous Correlations and Sampling Volume Considerations

Thus far, we have discussed the background of the Z vs P relationships, have indicated the several methods of computing Z, and have described how P and M are measured or derived at the ground level and aloft. Comment will now be made about the nature of the correlation and regression-analyses performed in the past and about some of the problems involving comparison sampling volumes.

Much of the previous correlation work which yielded particular regression or best-fit equations of Z vs P, as summarized in Section 2, was performed using Z and P values, both of which were computed from measurements (or presumed knowledge) of the size distribution properties of the hydrometeors. In other words, the Z and P values used to obtain the regression or best-fit equations [of the Eq. (1) type herein] were not independent values, rather they were interrelated through the commonality of the size-distribution data used for computations. Additionally, as discussed by Mason,[33] many of these equations were obtained from data acquired from sampling volumes of relatively small size, of the order of 0.1 to 1.0 m^3. This, Mason notes, probably contributes to the considerable differences among the equations reported in the literature. Mueller and Sims[34] have also discussed this problem.

---

*The Australian liquid-water-content meter is an instrument in which special electrolytic paper, on a roll, is exposed to the airstream, behind a slit. The impinging water droplets moisten the paper and change its conductivity, providing a measure of the liquid-water-content.

33. Mason, B. J. (1971) The Physics of Clouds, Second Edition, Clarendon Press, Oxford, England.

34. Mueller, E. A., and Sims, A. L. (1966) The influence of sampling volume on raindrop size spectra, Proc. 12th Weather Radar Conf., Norman, Oklahoma, p. 135 (479, 608).

The difficulty with small sampling volumes is that the largest hydrometeors, which exist in relatively small number concentration in the atmosphere (1 per m^3 to 1 per 100 m^3, or so) are either not represented or are inadequately represented in the sample. These largest hydrometeors do not contribute significantly to the liquid-water-content or precipitation rate, which are essentially functions of D^3, D being diameter, but they do contribute importantly to the reflectivity factor which is dependent on D^6. In fact, a few large hydrometeors may contribute more to the reflectivity factor than does the totality of all the other smaller hydrometeors. Thus, one must be exceedingly cautious, in the use of empirical Z vs P relationships, to insure that these were obtained from data samples of sufficient size to be representative of the pulse volume (or integration volume) of the radar.

It would seem that the Z vs P relationships of greatest validity would be those obtained from correlation analyses in which radar-measured values of Z [for a calibrated radar, see Eqs. (2) and (3)] were correlated with independent values of P, acquired from surface or aircraft measurements. Such studies, involving surface rainfall measurements, have been reported by Marshall et al,[3] Hooper and Kippax,[35] Hood,[36] Austin and Williams,[37] and Doherty.[38] These direct correlation investigations, however, have been relatively few in number, primarily because of the difficulties and uncertainties of radar calibration and proper pulse-volume-averaging, as noted by Austin.[39] Questions exist about the validity of various of the previous results.

4. THE AFCRL MEASUREMENT AND ANALYTICAL PROGRAM

The objectives of the AFCRL measurement-analytical program for the SAMS, Wallops Island storms may now be described.

35. Hooper, J. E. N., and Kipp , A. A. (1950) Radar echoes from meteorological precipitation, Proc. I. E. , 97(Pt. 1):89.

36. Hood, A. D. (1950) Quantitative measurements at 3 and 10 centimetres of radar intensities from precipitation, Nat. Res. Counc., Rpt No. 2155, Ottawa.

37. Austin, P. M., and Williams, E. L. (1951) Comparison of radar signal intensity with precipitation rate, M. I. T. Weather Radar Research, Tech. Rpt No. 14.

38. Doherty, L. H. (1963) The scattering coefficient of rain from forward scatter measurements, Proc. of the Tenth Weather Radar Conf., A. M. S., Boston, p. 171.

39. Austin, P. M. (1964) Radar measurements of precipitation rate, Proc. of the Eleventh Radar Conf.

The general objectives were to obtain observational and measurement information for each of the storms that would (1) define the hydrometeor types and regions that were present in the storms at the different levels, (2) establish the particular relationships among Z, P, and M that pertained to the observed hydrometeor types, (3) utilize these relationships to compute the M and P values corresponding to the radar-measured values of Z for the missile trajectories, and (4) also compute, or otherwise determine the size-distribution properties of the hydrometeors along the trajectories.

4.1 The Hydrometeor Regions

There are four identifiable hydrometeor regions that exist in the winter storms at Wallops Island which may be defined in terms of the type and size-distribution properties of the hydrometeors. These regions, from top to bottom of the storm, in the order of the progressive development of the hydrometeors, are (1) the ice-crystal region, (2) the small-snow region, (3) the large-snow region, and (4) the rain region. The hydrometeors in each of these regions may, in turn, be sub-classified on the basis of their particular characteristics. Thus, sub-classification in the ice-crystal region is made on the basis of the specific type of ice-crystals that are present as, for example, columns, plates, dendrites, or needles. In the snow regions, it is dependent on the predominant types of ice-crystals that are contained in and comprise the snow aggregates. In the rain region, it is made on the basis of the nature of the size-distribution of the raindrops.

The hydrometeor regions and sub-classes used in the SAMS program are identified in Table 2.

Not all of the hydrometeor regions are necessarily present in any given storm. If the storm has a convective nature, for example, and depending on how the SAMS missile traversed the storm, there may not be an ice crystal region at the top of a particular convective-element intercepted by the missile, or perhaps neither the ice crystal region nor small-snow region may exist in such a situation.

4.2 The Equations Used

Particular empirical equations of the types described in Sections 2 and 3 were used for each of the above hydrometeor regions to determine the values of P and M that corresponded to the radar-measured values of Z. Thus, P was computed from the equation

$$P = K_p Z^{E_p}, \tag{24}$$

which is an inversion of the traditional form of relationship of Eq. (1).

Table 2. Hydrometeor Regions and Types, Together With the Empirical Equations Relating P, Z, and M That Were Used for the SAMS Rain-Erosion Computations

Hydrometeor Region and Type	Symbol	(1) Equation Relating P and Z $\left(\text{i.e., } P=K_P Z^{E_P}\right)$	(2) Equation Relating M and P $\left(\text{i.e., } M=kP^{\ell}\right)$	(3) Equation Relating M and Z $\left(\text{i.e., } M=K_M Z^{E_M}\right)$	Obtained From
Ice Crystal Region					
Columns, Bullets, Rosettes	C_1	$P = .100\ Z^{.719}$	$M = .206\ P^{.735}$	$M = .038\ Z^{.529}$	Heymsfield data, Cunningham analysis
Needles	C_2	--	--	--	
Plates	C_3	--	--	--	
Graupel, Pellets	C_4	--	--	--	
Dendrites, Stellars	C_5	--	--	--	
Small-Snow Region					
Single-Crystal Snow	SS_S	$P = .0365\ Z^{.625}$	$M = .250\ P^{.860}$	$M = .0145\ Z^{.538}$	Marshall-Gunn[10] Equation, Cunningham modifications
Aggregates of Columns, Bullets	SS_1	--	--	--	
Aggregates of Needles	SS_2	--	--	--	
Aggregates of Plates	SS_3	--	--	--	
Aggregates of Graupel, Pellets	SS_4	--	--	--	
Aggregates of Dendrites, Stellars	SS_5	--	--	--	
Large-Snow Region					
Large Aggregates of Columns, Bullets	LS_1	$P = .0214\ Z^{.656}$	$M = .250\ P^{.941}$	$M = .00672\ Z^{.615}$	Ohtake data, Vardiman-Cunningham analysis
Large Aggregates of Needles	LS_2	$P = .0199\ Z^{.547}$	$M = .209\ P^{.872}$	$M = .00686\ Z^{.477}$	
Large Aggregates of Plates	LS_3	$P = .0169\ Z^{.631}$	$M = .233\ P^{.944}$	$M = .00495\ Z^{.596}$	
Large Aggregates of Graupel, Pellets	LS_4	$P = .0298\ Z^{.489}$	$M = .137\ P^{.805}$	$M = .00807\ Z^{.394}$	
Large Aggregates of Dendrites, Stellars	LS_5	$P = .00815Z^{.581}$	$M = .328\ P^{.906}$	$M = .00420\ Z^{.526}$	
Cunningham Snow*	LS_C	$P = .0311\ Z^{.454}$	$M = .254\ P^{.847}$	$M = .01345\ Z^{.385}$	
Rain Region					
Joss Drizzle	R_{JD}	$P = .0371\ Z^{.667}$	$M = .1075\ P^{.864}$	$M = .00624\ Z^{.576}$	Joss et al[40]
Joss Widespread	R_{JW}	$P = .0252\ Z^{.667}$	$M = .0756\ P^{.864}$	$M = .00314\ Z^{.576}$	Joss et al[40]
Joss Thunderstorm	R_{JT}	$P = .0159\ Z^{.667}$	$M = .0580\ P^{.864}$	$M = .00162\ Z^{.576}$	Joss et al[40]
Disdrometer, 3 February 1972	R_D	$P = .0181\ Z^{.698}$	$M = .0562\ P^{.910}$	$M = .00146\ Z^{.635}$	Wallops Is. Disdrometer Data
Disdrometer, 17 February 1972	R_D	$P = .0316\ Z^{.615}$	$M = .0664\ P^{.800}$	$M = .00419\ Z^{.490}$	Wallops Is. Disdrometer Data
Disdrometer, 17 March 1972	R_D	$P = .0293\ Z^{.675}$	$M = .0745\ P^{.846}$	$M = .00376\ Z^{.571}$	Wallops Is. Disdrometer Data
Disdrometer, 22 March 1972	R_D	$P = .0154\ Z^{.734}$	$M = .0595\ P^{.909}$	$M = .00134\ Z^{.667}$	Wallops Is. Disdrometer Data

*A type used only in the 1971-72 season.

The K_p and E_p values of this equation were specified for each of the hydrometeor regions and each hydrometeor type (where information existed). The particular values used for the data of the 1971-72 and 1972-73 SAMS seasons are listed in Table 2. The values for the rain region were obtained from disdrometer data and from the work of Joss et al.[40] The values for the snow and ice crystal regions were obtained by Cunningham from analyses that will be described in a subsequent report.

The Z values employed in the above equations, except for the surface and uppermost layers of the storm (these exceptions will be discussed), were the radar-measured values of Z_W, as specified by Eq. (2), for water hydrometeors, and Z_I, as specified by Eq. (3), for ice hydrometeors.

It was assumed, in all of the storm analyses, that the precipitation liquid-water-content was related to the precipitation rate in the manner described by Eq. (20) which, rewritten, is

$$M = kP^{\epsilon}, \tag{20}$$

where again the particular values of k and ϵ were specified for each hydrometeor region and type, as shown in Table 2.

It follows, from Eqs. (24) and (20), that the precipitation liquid water content is related, or implicitly assumed to be related, to the radar Z values as

$$M = K_M Z^{E_M}, \tag{25}$$

where

$$K_M = k K_p^{\epsilon} \tag{26}$$

and

$$E_M = \epsilon E_p . \tag{27}$$

The values of K_M and E_M for Eq. (25) were established for each hydrometeor region and type either (1) from knowledge of K_p, E_p, k and ϵ, using Eqs. (26) and (27), or (2) from regression analyses in which aircraft-determined values of M and Z, obtained from size distribution measurements, were inter-correlated. In either event, the consistency of the equation set, composed of Eqs. (24), (20),

40. Joss, J., Thams, J. C., and Waldvogel, A. (1968) The variation of raindrop size distributions at Locarno, Proc. Internatl. Conf. on Cloud Physics, Toronto, Amer. Meteorol. Soc., Boston, p. 369.

and (25), was maintained through use of the Eqs. (26) and (27). The details of these analyses will be described by Cunningham, as mentioned earlier. The particular K_M and E_M values determined from his analyses are shown in Table 2.

It will be noted, with reference to Table 2, that the coefficients and exponents are presented for only one of the ice crystal types listed and for only one of the small-snow types. This reflects the fact that AFCRL has not yet established the values for the other listed types. One of the prime objectives of the continuing SAMS program at AFCRL is the acquisition of appropriate, simultaneous radar and aircraft information that will permit the specification of the equation values for these other hydrometeor types (and that will also permit the accuracy verification of all equations for all hydrometeor types).

4.3 The Equations in Inverse Form

Most of the computations for the SAMS missile trajectories were performed using Eqs. (24), (20), and (25). However, occasional need also existed for computations employing the inverse form of the equations, in which the "independent" and "dependent" variables are reversed.* The constants and exponents of the equations in this form are presented in Table 3. These are the more or less traditional forms of the equations; hence their presentation facilitates comparisons with the equations of other investigators, as reported in the literature.

4.4 Reflectivity Factor Values for the Missile Trajectories

The radar values of the integration signal, $\bar{I}$, were determined for the major portions of the SAMS missile trajectories by methods described in the previous report by Plank.[1] (Subsequently, this report will be referred to as "R No. 1".) Special problems existed, however, in determining or estimating the $\bar{I}$ values that existed within two particular altitude layers within the storms, namely the surface layer and the highest layer.

Ground clutter return from the launch site location masked the hydrometeor echoes along the lowest portion of the missile trajectories (to about 0.4 km altitude), and it was necessary to assume that the $\bar{I}$ signals received from just offshore of the launch site (about 1.3 km offshore) were representative of those of the surface layer trajectories at the same altitudes.

The backscatter return from the hydrometeors along the trajectory portions near and at the storm top at the range extremity of the missile paths through the

*For example, the radar values of Z could not be obtained for the surface level point of the missile trajectory, because of ground clutter. Thus, for purposes of overall, computational consistency, the "effective values of Z" had to be determined from the surface measurements of P, which involved use of the "reverse-form equations" cited above.

Table 3. Inverse Form of the Equations of Table 2

Hydrometeor Region and Type	Symbol	Equation Relating Z and P	Equation Relating P and M	Equation Relating Z and M
Ice Crystal Region				
Columns, Bullets, Rosettes	C_1	$Z = 24.5\ P^{1.39}$	$P = 8.58\ M^{1.36}$	$Z = 484\ M^{1.89}$
Needles	C_2	--	--	--
Plates	C_3	--	--	--
Grauple, Pellets	C_4	--	--	--
Dendrites, Stellars	C_5	--	--	--
Small-Snow Region				
Single-Crystal Snow	SS_S	$Z = 200\ P^{1.60}$	$P = 5.00\ M^{1.16}$	$Z = 2620\ M^{1.86}$
Aggregates of Columns, Bullets	SS_1	--	--	--
Aggregates of Needles	SS_2	--	--	--
Aggregates of Plates	SS_3	--	--	--
Aggregates of Grauple, Pellets	SS_4	--	--	--
Aggregates of Dendrites, Stellars	SS_5	--	--	--
Large-Snow Region				
Large Aggregates of Columns, Bullets	LS_1	$Z = 354\ P^{1.53}$	$P = 4.36\ M^{1.06}$	$Z = 3410\ M^{1.63}$
Large Aggregates of Needles	LS_2	$Z = 1290\ P^{1.83}$	$P = 6.02\ M^{1.15}$	$Z = 34400\ M^{2.10}$
Large Aggregates of Plates	LS_3	$Z = 642\ P^{1.58}$	$P = 4.68\ M^{1.06}$	$Z = 7380\ M^{1.68}$
Large Aggregates of Grauple, Pellets	LS_4	$Z = 1320\ P^{2.04}$	$P = 11.80\ M^{1.24}$	$Z = 205000\ M^{2.54}$
Large Aggregates of Dendrites, Stellars	LS_5	$Z = 3950\ P^{1.72}$	$P = 3.42\ M^{1.10}$	$Z = 33000\ M^{1.90}$
Cunningham Snow*	LS_C	$Z = 2090\ P^{2.20}$	$P = 5.04\ M^{1.18}$	$Z = 72400\ M^{2.60}$
Rain Region				
Joss Drizzle	R_{JD}	$Z = 140\ P^{1.50}$	$P = 13.20\ M^{1.16}$	$Z = 6730\ M^{1.74}$
Joss Widespread	R_{JW}	$Z = 250\ P^{1.50}$	$P = 19.90\ M^{1.16}$	$Z = 22200\ M^{1.74}$
Joss Thunderstorm	R_{JT}	$Z = 500\ P^{1.50}$	$P = 27.00\ M^{1.16}$	$Z = 69900\ M^{1.74}$
Disdrometer, 3 February 1972	R_D	$Z = 314\ P^{1.43}$	$P = 23.70\ M^{1.10}$	$Z = 29200\ M^{1.57}$
Disdrometer, 17 February 1972	R_D	$Z = 278\ P^{1.63}$	$P = 29.70\ M^{1.25}$	$Z = 71200\ M^{2.04}$
Disdrometer, 17 March 1972	R_D	$Z = 187\ P^{1.48}$	$P = 21.50\ M^{1.18}$	$Z = 17600\ M^{1.75}$
Disdrometer, 22 March 1972	R_D	$Z = 295\ P^{1.36}$	$P = 22.30\ M^{1.10}$	$Z = 20300\ M^{1.50}$

*A type used only in the 1971-72 SAMS season.

storms were sometimes, in certain storms, below the minimum detectable by the radar. In such cases, the $\overline{I}$ values for the upper trajectory portions, that is, for the uppermost layer of the storms, had to be estimated. For storms of homogeneous structure, the assumption was made that the $\overline{I}$ values detected by the radar at vertical incidence would be representative of those of the missile trajectory in its upper portion.* For storms of convective structure, on the other hand, such an assumption could not be made, because of the spatial variability of the radar $\overline{I}$ values in the top part of the storm. The trajectory values, in this latter case, could merely be considered to be something smaller than the minimum detectable values at the particular range.

Aircraft observations and measurements were made in the Wallops storms during the periods immediately following the missile firings. These observations and measurements provided information (1) about the altitude boundaries and vertical extent of the melting zone, the hydrometeor regions and the transition zones within the storms, and (2) about the types and size-distribution properties of the hydrometeors in each region and zone.

Information was additionally available concerning the precipitation rate and size-distribution of the raindrops at the surface level (acquired from rain gauges and disdrometers) and concerning the vertical temperature and humidity structure of the storm (acquired from aircraft and special radiosonde measurements).

The aircraft information about the altitude boundaries of the melting zone permitted the differentiation of the regions of water and ice hydrometeors. This, in turn, permitted the reflectivity factors, Z_W and Z_I, to be computed from the trajectory values of the radar integration signal, $\overline{I}$. The procedures and equations used have been described in R No. 1. It was also noted in that report that both of the reflectivity factors, Z_W, for water, and Z_I, for ice, were computed across the melting zone itself.

4.5 Computations of Precipitation Rate and Liquid Water Content

The trajectory values of P and M were computed from the Z_W and Z_I values using the methods and assumptions described in the following sections. The description begins at the storm top level and continues, section by section within the text, for each of the hydrometeor regions and zones that is normally observed in a Wallops Island storm of homogeneous (non-convective) type. Thus the descriptive order follows that of the natural developmental processes that

*The radar at vertical incidence can detect the $\overline{I}$ signals from the storm top whereas the radar at the elevation angle of the missile trajectory cannot. The reason is that the radar range to the storm top is smaller at vertical incidence.

occur in the storm as the hydrometeors are generated and fall gravitationally through the depth of the storm to the surface level.

Comments about the observed nature of the regions and zones, and/or about particular computational problems, are made at the beginning of each section. The computation procedures used to obtain P and M are explained thereafter.

4.5.1 STORM TOP

The clouds at the upper boundaries of the storms, at the exit points of the SAMS missiles, were not reliably detected by the radar, at least not in the 1970 to 1973 seasons. Thus, the storm-top altitudes at the missile exit points had to be established either from aircraft observations, when aircraft, usually the AFCRL C-130, were present that could fly at these altitudes (of approximately 26,000 to 32,000 ft), or they had to be estimated from vertical-incidence radar data and/or from the humidity profiles or radiosonde ascents. Estimation accuracy, in the latter case, was probably about ±1000 ft or so for storms with uniform top structure, and was possibly no better than ±2000 ft to ±5000 ft for storms having convective top structure, dependent on the spatial organization and altitude variability of the convective elements.

The radar Z_W value, also the P and M values, were assumed to have zero values at the storm top level. This may be patently obvious, but is mentioned for completeness.

4.5.2 ICE CRYSTAL REGION

The uppermost portion of most of the Wallops storms (again excepting those of convective type) is comprised of populations of individual ice crystals which exist at altitudes above about 25,000 ft to 28,000 ft, where the temperatures are generally less than -25°C. These ice crystals are generated and developed in a supersaturated environment (with respect to ice) which is created by the uplift motions within the storm in general (see Weickmann,[41] Magono,[42] Borovikov,[43] Atlas,[44] Hobbs,[45] and Ono).[46] The ice crystals have various different shapes,

41. Weickmann, H. (1947 Die Eisphäse in der Atmosphäre, Library Trans. 273, Royal Aircraft Establishment, Farnborough, 96 pp.

42. Magono, C. (1953) On the growth of snowflakes and graupel., Scient. Rpt Yokohama Univ., Ser. 1, No. 2, p. 18(239, 241, 242).

43. Borovikov, A. M. (1953) Some results on an investigation of the structure of crystal clouds (in Russian) Trudy Tsentral. Acrolog. Obs. No. 12(247).

44. Hosler, C. L., Jensen, D. C., and Goldshlak, L. (1957) On the aggregation of ice crystals to form snow, J. Meteorol. 14:415(250).

45. Hobbs, P. V. (1969) Ice multiplication in clouds, J. Atmos. Sci. 26:315-318.

46. Ono, A. (1970) Growth mode of ice crystals in natural clouds, J. Appl. Sci. 27(4):649-658.

dependent on the temperature-humidity conditions of their formation. Numerous experimental investigations have been conducted to ascertain the specific crystal types that occur under different meteorological conditions; for example, see Ludlam,[47] Nakaya,[48] Gold and Power,[49,50] Hosler,[51] Magono and Lee,[52] and Kikuchi.[22]

The generally-observed, most-common types of ice crystals are identified in Table 2.

The P and M values for those portions of the missile trajectories that passed through the ice crystal region were computed from the radar Z_I values using the equations shown in Table 2. Thus, P was first computed from Z_I, employing the equation of the first column, and M was then computed from P, utilizing the equation of the second column. The reason for computing P first is related to the transition-zone, interpolation problem discussed in the following section. Actually, however, the computational order is unimportant, since the equations of Table 2 are self consistent for each of the hydrometeor types.

Only one set of equations for ice crystals is presented in Table 2, which pertains specifically to ice crystals consisting of columns, bullets, and rosettes. These equations, as mentioned earlier, are the only ones presently available. Consequently, they had to be used commonly for all of the trajectory computations of P and M in the ice crystal region, irrespective of the actual crystal types observed in the Wallops storms.

4.5.3 ICE-CRYSTAL TO SMALL-SNOW TRANSITION ZONE

As the largest ice crystals in the uppermost part of the storm (those which have greater fall velocities than the other smaller, more-numerous crystals of the populations) descend through the supersaturated environment of the storm, they grow, presumably both by diffusion and by colliding with and "cohesively capturing various of the other smaller ice-crystals along their fall trajectories.

47. Ludlam, F. H. (1947) The forms of ice clouds, Quart. J. Roy. Meteorol. Soc. 74:39-56.

48. Nakaya, J. (1951) The formation of ice crystals, Compendium of Meteorol., Boston, Amer. Meteorol. Soc. 207-220.

49. Gold, L. W., and Power, B. A. (1952) Correlation of snow-crystal type with estimated temperature of formation, J. Meteorol. 9:447 (246-7).

50. Gold, L. W., and Power, B. A. (1954) Dependence of the forms of natural snow crystals on meteorological conditions, J. Meteorol. 11:35 (247).

51. Hosler, C. L. (1954) Factors governing the temperature of ice-crystal formation in clouds, Proc. Toronto Met. Conf., 1953, p. 253, R. Met. Soc., London (157).

52. Magono, C., and Lee, C. W. (1966) Meteorological classification of natural snow crystals, J. Fac. Sci., Hokkaido Univ. 2(Ser. VII):321-335.

The precise growth mechanisms are not clearly known, but aircraft measurements and observations indicate that the largest ice crystals do progressively grow and develop into "agglomerates", or "small snow" particles. [Theoretical and experimental information concerning aggregation processes have been reported by Magono,[42,53] Marshall and Langleben,[54] Hosler et al,[44] Nakaya et al,[55] Hosler and Hallogren,[56] and Podzimek.[57]]

The altitude zone in the storm in which this aggregation process is most pronounced [as observed by aircraft (see footnote below)] is herein defined to be "the ice-crystal to small-snow transition zone".* Seemingly, this is a physically-real zone, which separates the region of ice crystals aloft from the small-snow region below. The zone is bounded at the top at some upper level, where small single ice-crystals predominate within the populations, and only an occasional aggregate is observed which contributes insignificantly to the liquid-water-content of the populations.** The zone extends downward to some lower level, where aggregates are observed to be present in numbers such that they are the prime contributors to the liquid-water-content of the populations.

The precipitation rate (P) and liquid-water-content (M) values for the missile trajectory segments crossing this "ice-crystal to small-snow transition zone" were computed as follows:

The precipitation rate was assumed to be linearly variable through the zone, increasing downward. Thus,

$$P_d = P_{C_B} + \alpha_3 d, \tag{28}$$

53. Magono, C. (1957) On snowflakes, Proc. Sixth Wea. Radar Conf., pp. 31-36, Boston, Am. Meteorol. Soc.

54. Marshall, J. S., and Langleben, M. P. (1954) A theory of snow-crystal habit and growth, J. Meteorol. 11:104 (254-6).

55. Nakaya, U., Hanajima, M., and Muguruma, J. (1958) Physical investigations on the growth of snow crystals, J. Fac. Sci., Hokkaido Univ., Ser. II, 5, 87 (265).

56. Hosler, C. L., and Hallgren, R. E. (1961) Ice crystal aggregation, Nubila 4: 13 (249).

57. Podzimek, J. (1968) Aerodynamic conditions of ice crystal aggregation, Proc. Internatl. Conf. Cloud Phys., Toronto, 295-299.

The presence of aggregates in a population of ice crystals can be detected from aircraft (1) by seeing them occasionally strike the "snow-stick" instrument aboard the aircraft, (2) by seeing them "pass by" a black background, such as an engine nacelle, or (3) by detecting the occasional presence of "larger than ordinary" particles using the "raindrop spectrometer" instrument of the AFCRL C-130A aircraft.

**These statements may be clarified somewhat by pointing out that in almost all hydrometeor populations (composed of ice-crystals, or of snow, or of rain), the smallest particles or drops are the most numerous ones; see the size-distribution discussion of Section 7. Thus, the zone-boundary definitions above are "verbally awkward" because they refer to the "third moment properties" of the size spectra of the hydrometeors. If the definitions are bothersome, it is suggested that the reader turn directly to Section 7.

where P_d is the zone precipitation rate at the distance d below the base of the ice crystal region, where P_{C_B} is the precipitation rate at the base of the ice crystal region and

$$\alpha_3 = \frac{P_{SS_T} - P_{C_B}}{H_3} , \tag{29}$$

where P_{SS_T} is the precipitation rate at the top of the small-snow region (computed as indicated in the following section) and H_3 is the total vertical depth of the transition zone. The subscript "3" on α and H indicates that this transition zone is the third such zone above the surface level, as will be explained.

This assumption implies that the volume flux of water mass across horizontal surfaces within the transition zone is increasing linearly with the fall distance of the hydrometeor particles.* This is consistent with the progressive, downward development of the precipitation process within the storm.

The liquid-water-content values in this transition zone were computed from the Pd values using the equation

$$M_d = \left(\kappa_c + \beta_3 d\right) P_d^{\left(\epsilon_c + \gamma_3 d\right)} . \tag{30}$$

where M_d is the liquid-water-content at the distance d below the base of the ice crystal region and where k_c and ϵ_c are the coefficient and exponent of Eq. (20), which have the particular values pertaining to ice crystals, as listed in Table 2, column 2. The factors β_3 and γ_3 are given by

$$\beta_3 = \frac{k_{SS} - k_c}{H_3} \tag{31}$$

and

$$\gamma_3 = \frac{\epsilon_{SS} - \epsilon_c}{H_3} , \tag{32}$$

where k_{SS} and ϵ_{SS} are the coefficient and exponent of Eq. (20) that pertain to small-snow, as also specified in Table 2, column 2.

*The assumption that P is linearly variable with altitude is considered to be more physically realistic than the alternate possible assumption, which is that M is linearly variable. This is because the liquid-water-content in storms may be "held in storage", at any given level by two mechanisms: (1) by the different fall velocities of the constituents of hydrometeor populations of different type and (2) by the presence of updraft-downdraft motions within the storms. An assumption that P varies linearly, on the other hand, since P is a flux parameter, only involves the second mechanism. The detailed reasons are left unstated.

Thus, the values of M_d in the transition zone were computed under the assumption of the linear altitude variation of k and ϵ of Eq. (20). *

4.5.4 SMALL-SNOW REGION

The small-snow region, as the name indicates, is defined primarily on the basis of the size of the observed snow particles. This region extends downward from the base of the transition zone, described in the previous section, to some lower level where aircraft measurements indicate that the equivalent melted diameter of the largest snow aggregates is about 0.5 mm (which corresponds to physical sizes, dependent on snow type, ranging from approximately 1 to 3 mm).

Thus, small-snow and the small-snow region are defined in terms analogous to those used to define "drizzle" in the case of water hydrometeors. The maximum equivalent-melted-diameter specified for small-snow is the same as the maximum actual diameter for drizzle droplets, as drizzle is conventionally defined; see Huschke,[58] for example.

The P and M values for the trajectory segments that passed through the small-snow region were computed from the equations of the first and second columns of Table 2. The only equations available for small-snow at present are those of Marshall and Gunn[10] as modified by Cunningham (see Tables 2 and 3). These had to be used commonly for all storm computations of the past SAMS seasons.

4.5.5 SMALL-SNOW TO LARGE-SNOW TRANSITION ZONE

The distinction between the small-snow and large-snow regions in the Wallops storms was made on rather tentative and hypothetical grounds. Likewise, the definition of the transition zone between these regions was provisional and conjectural.

Observations and measurements obtained by the AFCRL C-130A aircraft in the Wallops storm of 2 February 1973 suggest that some "rapid growth process" occurred in the populations of falling snowflakes when the particles had attained maximum sizes of about 1 to 3 mm (about 0.5 mm equivalent melted diameter). When the aircraft flew at levels below the altitude where these sizes occurred, it was observed that the maximum-size particles seemingly became "much larger"

58. Huschke, R. E. (1959) Glossary of Meteorology, Amer. Meteorol. Soc., Boston, Mass.

*It might be argued, in view of the power function form of Eq. (20), that it would be preferable to assume a logarithmic variation of k with altitude, rather than linear. Practically, however, these different assumptions do not change the computed M_d values significantly (relative to the inherent uncertainties of the overall analyses).

by a factor of two or so within a relatively-small descent distance of a few thousand feet. The number density of these new, larger particles also increased downward.

Such observations suggest that some "quantum-type" of growth process might have been occurring in which the largest snowflakes were themselves colliding and "sticking together" to form conglomerates that were as much as twice as large as those existent at slightly higher altitudes.* It is also suspected that liquid water droplets (cloud droplets) might have been present in the storm at these altitudes which would cover the falling, tumbling snowflakes with a thin outer coating of liquid-water, freezing-water, or rime. Such coatings would greatly enhance the cohesion of these snowflakes following collisions.

Based on these observations and hypotheses, large-snow was tentatively defined to consist of populations of snow particles having maximum particle sizes exceeding 1 mm equivalent-melted-diameter (corresponding to physical sizes ranging from about 2 to 6 mm).

With this definition, and with that for small-snow previously stated, the transition zone separating the storm regions of small-snow aloft from large-snow below also became defined.** Thus, the transition zone became the particular growth layer in the storm in which the maximum particle sizes of the falling snow increased from 0.5 to 1 mm, in equivalent-melted-diameter, or from physical sizes ranging from about 1 to 3 mm, dependent on snow type, to sizes ranging from about 2 to 6 mm.

The computations of P and M for the portions of the missile trajectories that intersected the transition zone between small-snow and large-snow were performed in a manner analogous to that described in Section 4.5.3. The precipitation rate was assumed to be linearly variable with altitude and to be given by

---

*This does not imply that collisions were restricted only to the largest snowflakes. Rather, it implies that observational concentration was devoted primarily to these particular flakes within this zone.

**There are pragmatic reasons, in addition to any attempted physical justification, for specifying storm regions of small-snow and large-snow, together with a transition zone. The size-spectrum variability of snow in general is simply too large to permit accurate computations of P and M from empirical equations of the Table 2 type without some size categorization, such as the two-region categorization defined herein. The transition zone is necessary to prevent computational discontinuities of P and M, such as would result across the boundary between regions in the absence of a transition zone. What is really needed to resolve certain of these difficulties with snow is the acquisition by snow-type of equation sets relating P, Z, and M, which properly reflect the functional dependence of these parameters on the size-spectrum range of the snow particles. We do not have such equations at present, nor the data that would permit their obtainment.

$$P_d = P_{SS_B} + \alpha_2 d, \tag{33}$$

where P_d and d are as previously specified, where P_{SS_B} is the precipitation rate at the base of the small-snow region and

$$\alpha_2 = \frac{P_{LS_T} - P_{SS_B}}{H_2}, \tag{34}$$

where P_{LS_T} is the precipitation rate at the top of the large-snow region and H_2 is the total vertical depth of the transition zone.

The M_d values were computed from the P_d values using the equation

$$M_d = \left(k_{SS} + \beta_2 d\right) P_d \left(\epsilon_{SS} + \gamma_2 d\right) \tag{35}$$

where k_{SS} and ϵ_{SS} are the coefficient and exponent of Eq. (20), that have the Table 2, column 2, values pertaining to small-snow where

$$\beta_2 = \frac{k_{LS} - k_{SS}}{H_2}, \tag{36}$$

$$\gamma_2 = \frac{\epsilon_{LS} - \epsilon_{SS}}{H_2}, \tag{37}$$

and where k_{LS} and ϵ_{LS} are the constant and exponent of Eq. (20) having the Table 2, column 2, values corresponding to the type of large snow observed in the Wallops storms.

4.5.6 LARGE-SNOW REGION

The definition of large-snow was stated previously. The large-snow region extended downward from the base of the transition zone just discussed to the storm level at which the falling snowflakes first began to melt. The base of the snow region, in other words, was the altitude of the 0°C isotherm, or very nearly.

The P and M values for the missile trajectory segments that passed through this region were computed from the Table 2 equations for the observed snow type.

4.5.7 MELTING ZONE

The upper boundary of the melting zone was specified to be the storm level at which the snowflakes first began to melt. The lower boundary was designated to be the level at which all melting was complete, and below which only water-hydrometeors (rain) existed.

Dependent on the temperature structure of any given storm, it is sometimes possible to have two or more melting zones. Sandwiched layers of above-freezing and below-freezing temperatures can cause alternate melting, refreezing, and remelting of the snow-ice particles. Such multiple zones are not commonly observed but do occur occasionally, as in the case of the Wallops storm of 17 February 1972.

The melting zone is customarily detected by the Wallops Island radars (the FPS-18, Spandar, and the X band).* The zone, on RHI (range height indicator) scope presentations, appears as a distinctive "bright band". This bright band occurs because the snowflakes become water-coated during melting and reflect microwave energy as if they were large water particles of snowflake size. The enhanced radar return is explained by the fact that the reflectivity of liquid water at microwavelengths is substantially (about 5 times) larger than that for ice.

As noted in R No. 1, the radar volume reflectivity, η, is measurable in the melting zone, but the radar reflectivity factor, Z, is indeterminate.

The P and M computations for the melting zone were performed using equations similar to those for the other transition zones.
Thus,

$$P_d = P_{LS_B} + \alpha_1 d , \tag{38}$$

$$M_d = \left(k_{LS} + \beta_1 d\right) P_d^{\left(\epsilon_{LS} + \gamma_1 d\right)} , \tag{39}$$

$$\alpha_1 = \frac{P_{R_T} - P_{LS_B}}{H_1} , \tag{40}$$

$$\beta_1 = \frac{K_R - K_{LS}}{H_1} , \tag{41}$$

and

$$\gamma_1 = \frac{\epsilon_R - \epsilon_{LS}}{H_1} , \tag{42}$$

where P_d, M_d and d are as previously defined, where P_{LS_B} and P_{R_T} are the precipitation rates at the base of the large-snow region and at the top of the rain region, respectively, where H_1 is the vertical depth of the melting zone, and where K_{LS} and ϵ_{LS} are the coefficient and exponent of Eq. (20) that have the particular values listed in Table 2, column 2, for the observed type of large-snow.

*The melting zone is sometimes not detected if the storm has internal convective structure consisting of cells of updraft and downdraft motions.

4.5.8 RAIN REGION

The rain region extended downward from the base of the melting zone to the surface level. Rain was invariably present at the surface level in all Wallops storms to date into which SAMS missiles have been fired.

The P and M computations for the missile trajectory segments crossing the rain region were handled differently than in the other hydrometeor regions discussed previously. The principal factor of difference was that the size distribution properties of the rain at the surface level were measured, for each individual storm, by disdrometer instruments located at or near the launch site of the missiles. Thus, from the measurements of P, M, and Z (described in R No. 1), the particular P vs Z, M vs P, and M vs Z equations could be established by correlation and regression analyses for each storm for which reliable, quantitative disdrometer data had been acquired.

The equations obtained for the storms of the 1971-72 season of SAMS operations are presented in Table 2 at the bottom. These equations were used in the P and M computations for the rain region in the 1971-72 season. The equations of Joss et al,[40] for widespread rain (see Table 2) were used for the rain region computations of the 1972-73 season.*

4.5.9 SURFACE LEVEL

The precipitation rate at the surface level at the launch time(s) of the missile(s) was measured directly by means of a tipping-bucket rain gauge located near the launch site. This was the value of P used at the surface level.

The corresponding M value at the surface level was computed from Eq. (20), using the "disdrometer values" of k and ϵ of Table 2 for the storms of the 1971-72 seasons, and using the Joss values for widespread rain for the storms of the 1972-73 season.

4.6 Trajectory Computations from the Surface Upward

Because of the need to compute the integrated amounts of liquid water that were intercepted by the missiles as a function of their travel distance from the launch pad along the trajectories, the transition zone equations of Sections 4.5.3, 4.5.5, and 4.5.7 had to be written in modified form, such that the P and M values were specified in terms of distance measured upward from the base of the

*The equations obtained for the 1970-71 season are unknown to the author. Those for the 1972-73 season are available, but because of the data interpretation problems cited in R No. 1, they were obtained too late for application to the P and M computations for the 1972-73 season. These latter equations are not listed in Table 2.

zones, rather than downward from the top. The P and M equations for the first transition zone above the surface, the melting zone, were therefore rewritten as

$$P_h = P_{R_T} - \alpha_1 h \tag{43}$$

and

$$M_h = \left(k_R - \beta_1 h\right) P_h^{\left(\epsilon_R - \gamma_1 h\right)}, \tag{44}$$

where h is distance measured upward from the base of the zone, where α_1, β_1, and γ_1 are as specified, respectively, by Eqs. (40), (41), and (42), and where the other parameters are as previously defined.

Analogously, the equations for the second and third transition zones above the surface were modified to

$$P_h = P_{LS} - \alpha_2 h \tag{45}$$

and

$$M_h = \left(k_{LS} - \beta_2 h\right) P_h^{\left(\epsilon_{LS} - \gamma_2 h\right)}, \tag{46}$$

for the small-snow to large-snow transition zone, and to

$$P_h = P_{SS} - \alpha_3 h \tag{47}$$

and

$$M_h = \left(k_{SS} - \beta_3 h\right) P_h^{\left(\epsilon_{SS} - \gamma_3 h\right)}, \tag{48}$$

for the ice-crystal to small-snow transition zone, where h, as before, is distance measured upward from the base of the zones and α_2, β_2, γ_2, α_3, β_3, and γ_3 are specified by Eqs. (34), (36), (37), (29), (31), and (32), respectively. The other parameters were defined earlier.

4.7 Integral of Liquid-Water-Content Along the Missile Trajectory

The equations described in the preceding sections permitted the computation of P and M for the SAMS missile trajectories.

With knowledge of M, additional computations were performed to provide information about the "trajectory integral" of M as a function of the path distance, R_S, from the missile launch pad. Thus, the values of

$$\int_0^{R_S} M dR_S = \sum_0^{i=n} \overline{M}_i \, \Delta R_{S_i} \, , \tag{49}$$

were computed for each radar (or interpolated) data point along the trajectory as a function of the path distance

$$R_S = \sum_0^{i=h} \Delta R_{S_i} \, . \tag{50}$$

In these equations, ΔR_{S_i} is the incremental distance between the successive data points, which are numbered from i=1 to i=n along the trajectory, and $\overline{M}_i$ is the average liquid-water-content between the successive points. The summation is accomplished cumulatively, from data point to data point, up to the storm top level.

4.8 Profile Values of the Hydrometeor Parameters

The trajectory values of P and M were tabulated and plotted as a function of the altitude, z, of the data points above the surface level. These tabulations and plots, with z as the vertical coordinate, will be referred to herein as the "profile values" or "profile plots". This method of tabulation and plotting facilitates comparisons of the erosion conditions encountered by the different missiles launched into the different storms.

With regard to the profile values of the integral of liquid-water-content, an assumption was made regarding the relationship between the trajectory distance between data points, ΔR_S, and the altitude distance (component distance) between the same points, Δz. These increments are related as

$$\Delta R_S = \csc \phi \, \Delta z \, , \tag{51}$$

where ϕ is the elevation angle of the missile trajectory above the horizontal plane in the vicinity of the data points.

This equation substituted in Eq. (49) yields

$$\int_0^{R_S} M dR_S = \sum_0^{i=n} \overline{M}_i \, (\csc \phi)_i \, \Delta z_i \, , \tag{52}$$

which permits the integral on the left to be determined as a profile function of the altitude

$$z = \sum_{0}^{i=n} \Delta z_i \,, \tag{53}$$

rather than as a function of the path distance, R_S, as formerly with Eqs. (49) and (50).

The trajectories of the Terrier-Recruit missiles used in the SAMS program of the 1970-73 seasons, the portions between the surface and storm top altitudes, can be approximated quite well by a straight line having an average elevation angle, $\bar{\phi}$. This permits Eq. (52) to be written as

$$\int_0^{R_S} M dR_S \cong \csc \bar{\phi} \sum_{0}^{i=n} \bar{M}_i \, \Delta z_i \,. \tag{54}$$

For the five SAMS missiles fired during the 1971-72 season, the average elevation angle of the straight lines of "best-fit approximation" to the actual trajectories was 29.3°. This value, inserted in Eq. (54), for $\bar{\phi}$, yields

$$\int_0^{R_S} M dR_S \cong 2.04 \sum_{0}^{i=n} \bar{M}_i \, \Delta z_i \,. \tag{55}$$

The above equation was used to compute the profile values of $\int_0^{R_S} M dR_S$ for both the 1971-72 and 1972-73 seasons of SAMS operations. The values of the integral thus computed should not depart by more than about 5 percent at the storm top level of maximum value from those computed from the more rigorous Eqs. (49) and (50).

5. COMPUTATIONAL EXAMPLE

A typical example has been selected that will serve to summarize and illustrate the computational procedures described in the preceding sections. The particular example is the missile flight, No. Q2-6361, of 2 February 1973, launched at 1408:30 GMT.

The trajectory values of the radar integration signal, $\underline{\bar{I}}$, for this flight are shown in Figure 1 as a function of altitude; see the upper abcissa scale.* The solid, middle portion of the profile shows the radar-measured values of $\underline{\bar{I}}$ for the trajectory portion extending from just above the ground clutter region near the

*The "bracket underline" symbol, "$\underline{\ }$", is used, as in R No. 1, to specify the decibel-equivalent value of any given parameter. Thus, $\underline{\bar{I}} = 10 \log \bar{I}$.

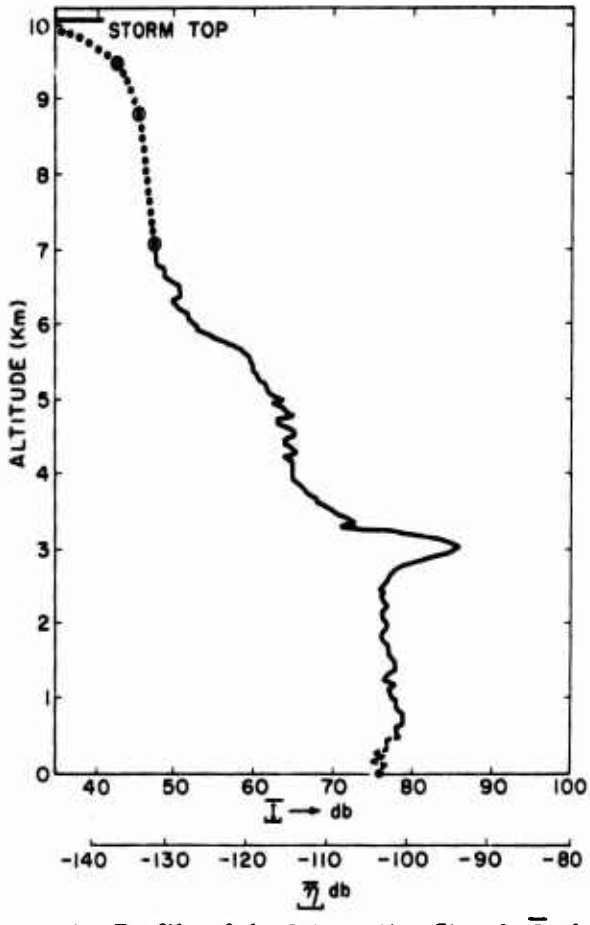

Figure 1. Profile of the Integration Signal, $\overline{I}$, for the Storm Trajectory of Missile Q2-6361, of 2 February 1973. The associated decibel values of radar volume reflectivity, $\overline{\eta}$, are indicated by the second abscissa scale. The solid, dashed and dotted portions of the profile are explained in the text

surface level to the storm altitude where the $\overline{I}$ value became smaller than the minimum detectable value of the radar.

The dashed portion of the profile, at the bottom, shows the $\overline{I}$ values measured along a vertical line located about 1.3 km offshore of the missile launch site, where ground clutter effects were absent or minimized, relative to those at the launch site. The values were presumed to be representative of the trajectory values.

The dotted portion of the Figure 1 profile, at the top, shows the $\overline{I}$ values that were assumed to apply to the uppermost part of the missile trajectory. The data point at 8.8 km altitude, for which $\overline{I}$ = 45.5 db, was obtained by "special processing" of the radar data recorded at the launch time of the missile. The radar signal

values for a 1° sector of the RHI scan, for an elevation angle of approximately 30°, were integrated over the sector, for each and all pulse-volume ranges in the upper portion of the storm, to establish the minimum detectable value of the integral and the associated storm altitude.* This technique, in essence, employs integration to determine the values of "weak signals" that are "obscured by" receiver noise. The data point cited above was ascertained by this technique.

The storm top altitude on 2 February 1973 was 10.1 km, as established by observation from the AFCRL C-130 aircraft. The $\bar{I}$ value at the storm top was assumed to be unity (that is, $\underline{I} = 0$), and the $\bar{I}$ values between data points in the upper portion of the storm were assumed to be linearly variable with altitude.**

The $\underline{I}$ value at the surface level, specifically emphasized in Figure 1 by the large black dot, was inferred from the precipitation rate measured by the tipping-bucket rain gauge at the launch site at the firing time of the missile.†

The lower abscissa scale in Figure 1 shows the decibel values of the radar volume reflectivity, $\underline{\eta}$, that correspond to the $\underline{I}$ values. $\underline{\eta}$ and $\underline{I}$ are related, as specified by Eq. (47) of R No. 1.

Aircraft measurements during the storm of 2 February 1973 established that the base and top of the melting zone were located at altitudes of about 2.7 and 3.7 km, respectively. This information permitted the values of the reflectivity factor for water hydrometeors, Z_W, and those for ice hydrometeors, Z_I, to be computed from the $\underline{I}$ values of the Figure 1 profile, utilizing Eqs. (72) and (73) of R No. 1. The resultant profiles of Z_W and Z_I for the missile trajectory are shown in Figure 2. The separate profiles have been extended across the melting zone itself. The values of the reflectivity factor are indeterminant within the zone, as mentioned earlier. The values should generally exceed those of the Z_I profile, but the amount of the excess is impossible to predict without making theoretical assumptions about the nature of the melting processes in this particular storm.

The aircraft measurements and observations also provided information about the upper levels of the storm. The large-snow in the region immediately above

---

*The maximum elevation angle of the RHI scans during the storm of 2 February 1973 was about 30°.

**This assumption was used for the 1972-73 SAMS data. However, the assumption that $\underline{I}$ was linearly variable was used for the 1971-72 data. It should be noted that if $\bar{I}$ varies linearly with altitude, $\underline{I}$ does not, and vice versa. This explains the curvature of the Figure 1 profile between the circled data points above 7 km altitude.

†In other words, to complete the profile, the $\underline{I}$ value for the surface level was "back calculated" from P, first utilizing the Z vs P relationship of Joss et al.[29] for widespread rain, as listed in Table 3, column 1, and then employing the $\underline{I}$ vs Z relationship of Eq. (72) of R No. 1.

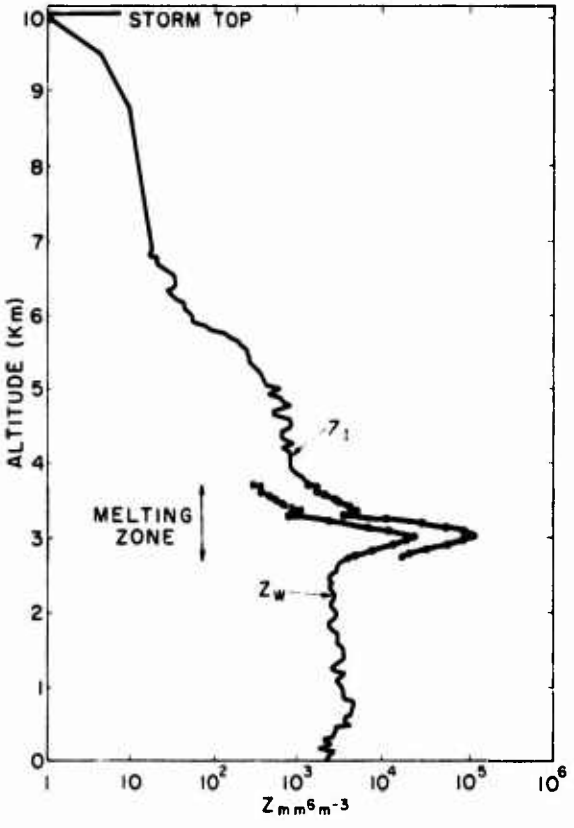

Figure 2. Profiles of the Radar Reflectivity Factors, Z_W, for Water Hydrometeors, and Z_I, for Ice Hydrometeors, for the Missile Trajectory

the melting zone was composed primarily of "aggregates of plates". The base and top of the small-snow to large-snow transition zone were located at altitudes of about 5.9 and 6.8 km, respectively. The base and top of the ice-crystal to small-snow transition zone were located at about 8.0 and 8.5 km, respectively. These hydrometeor regions and transition zones are illustrated in Figure 3.

Also illustrated in Figure 3 is the profile of precipitation rate for the missile trajectory. The P values for the identified hydrometeor regions and types were computed from the Z_W and Z_I values of the Figure 2 profiles using the pertinent equations of Table 2, column 1. The P values within the transition zones were assumed to be linearly variable with altitude as previously discussed, and as is revealed in Figure 3 by the straight-line segments shown crossing the zones.

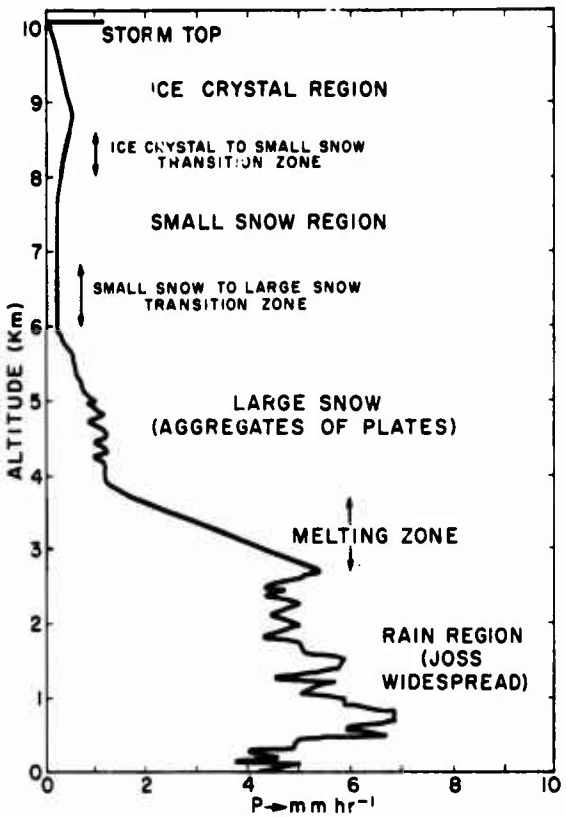

Figure 3. The Hydrometeor Regions and Zones Within the Storm and the Profile of Precipitation Rate, P

The M values for the missile trajectory are illustrated by the solid-line profile of Figure 4. These M values for the different regions and zones were computed from P using the applicable equations of Table 2, column 2, within regions, and the interpolation equations of Section 4.6 within zones.

The dashed curve of Figure 4 shows the profile of $\int M\, dR_S$. The values of this integral were determined from the M values, using Eqs. (53) and (55) of Section 4.8. The maximum value of the integral for the entire storm passage distance of the missile is indicated by the drafted number at the top of the profile. The units of the integral are gm m^{-2}.

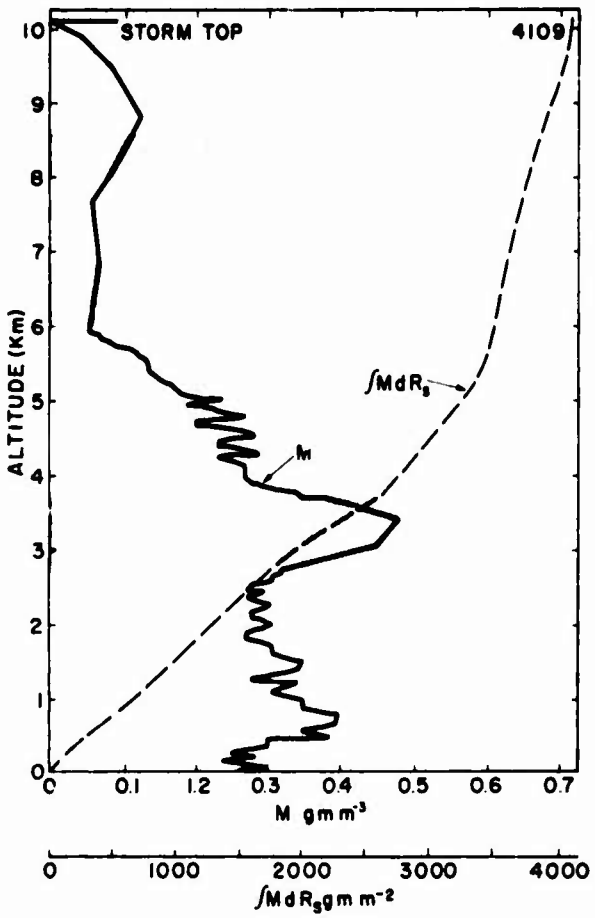

Figure 4. Profiles of Liquid-Water-Content, M, and Integral of Liquid-Water, $\int M\, dR_s$, for the Missile Trajectory

6. UNCERTAINTIES

The erosion parameters of prime importance to the SAMS program at Wallops Island are the profile values of M and $\int M\, dR_s$. It follows, then, that questions concerning the uncertainties and error bounds of these two parameters are also of major interest.

The uncertainties and indeterminacies of the radar-measured values of Z_W and Z_I were discussed in R No. 1 in Appendix B. These uncertainties, for the SAMS conditions of radar operation (with the FPS-18 radar) during the 1971-72 and 1972-73 seasons, were suggested to be of the order of ±50 percent to ±65 percent, for 8 range-cell integration, dependent on the estimates made regarding the uncertainties of the individual contributing factors.

It has been shown herein that the M values for the missile trajectories were derived from the radar-measured values of Z, either Z_W or Z_I, using empirical equations of the types listed in Table 2. The equation that specifies the direct dependence of M on Z is Eq. (25), which, rewritten, is

$$M = K_M Z^{E_M} . * \tag{25}$$

This equation shows that the uncertainties of M will depend on the component uncertainties of each of the right-hand factors, Z, K_M, and E_M.**

The total variation of M resulting from component variation of Z, K_M, and E_M is given by

$$dM = \frac{\partial M}{\partial Z} dZ + \frac{\partial M}{\partial K_M} dK_M + \frac{\partial M}{\partial E_M} dE_M , \tag{56}$$

which, when the partial derivatives are evaluated from Eq. (25), becomes

$$dM = K_M Z^{E_M} \left(\frac{E_M dZ}{Z} + \frac{dK_M}{K_M} + \ln Z \, dE_M \right). \tag{57}$$

The derivatives d_Z, dK_M, and dE_M of this equation may be identified and associated with the uncertainty variations of the parameters Z, K_M, and E_M.

The possible magnitude of these uncertainties will be discussed in the following sections, and estimates will be made of the associated uncertainties of liquid-water-content.

Two kinds of situations are postulated for uncertainty estimation. In the first, which will subsequently be referred to as "Situation 1", it is assumed that only radar-measurement data are available and that auxiliary surface and aircraft data are not (except for knowledge of the general category of the hydrometeors; that is, whether they are rain, snow, or ice crystals). In "Situation 2", in contrast, both types of data are presumed to have been acquired.

---

*The fact that M, in the profile computations just discussed, was computed from Eqs. (20) and (24), rather than from Eq. (25), does not negate this statement. The equation sets of Table 2 are self-consistent, and the M values computed by either procedure will be identical (within two-place accuracy).

**Since Eq. (25) is an empirical equation, questions can be raised whether some different form of equation, other than a power function, might be more descriptive of the data, hence more accurate. Such questions are valid, but they are beyond the scope of the present report. The uncertainty comments of this section are based on the assumption that Eq. (25) is the best descriptive equation presently available.

6.1 Estimated Uncertainties of Liquid-Water-Content for Rain and Large-Snow Under Situation 1

In Situation 1, with reference to Eq. (57), the dM uncertainties of liquid-water-content will depend on four component uncertainties: (1) on the dK_M uncertainties of our knowledge of the proper constant of Eq. (25) that should be applied to the given hydrometeor category; (2) on the dE_M uncertainties of our knowledge of the proper exponent; (3) on the dZ uncertainties of radar measurement that were discussed in R No. 1; and (4) on the dZ uncertainties that reflect the scatter of the Z values, used in the regression analyses, about the regression line obtained from the analysis. Thus, with regard to the latter two components, the dZ parameter of Eq. (57) is actually composed of two parts,

$$dZ = dZ_{rm} + dZ_S , \tag{58}$$

where dZ_{rm} is the uncertainty of the radar-measured values of Z and dZ_S is the uncertainty, or "scatter", of the Z values used in the regression analyses about the regression line.

When Eq. (58) is substituted in Eq. (57), we obtain the general form of the uncertainty equation for M, that is,

$$dM = K_M Z^{E_M} \left[\frac{E_M}{Z} \left(dZ_{rm} + dZ_S \right) + \frac{dK_M}{K_M} + \ln Z \, dE_M \right] . \tag{59}$$

In evaluating this equation for the Situation 1 presumption, it will be advantageous to discuss the dK_M and dE_M component uncertainties first. We will then review and retabulate certain of the dZ_{rm} information from R No. 1. Finally, we will consider the dZ_S uncertainties and present the equation-evaluation results.

The ranges of the K_M and E_M values for rain and large-snow are shown from the equations of Table 2, column 3. In lieu of knowledge of the specific rain or large-snow type, which is the Situation 1 presumption, it would seem that we would be subject to K_M and E_M variability at least as large as the ranges shown in this table.

The Table 2 equations for rain (the disdrometer and Joss equations) reveal that K_M varies from 0.00134 to 0.00624, with an arithmetic mean value of 0.00311 and a standard deviation of ± 0.00167. The E_M values range from 0.490 to 0.667; the arithmetic mean is 0.585; the standard deviation is ± 0.0516.

For large-snow, the Table 2 equations show that K_M varies from 0.00420 to 0.00807, with a mean of 0.00616 and standard deviation of ± 0.00140. The E_M values range from 0.394 to 0.615; the mean is 0.522; the standard deviation is ± 0.0807.

It was assumed, for the purposes of uncertainty estimation, that the K_M and E_M values of Eq. (59), for rain and large-snow, would be given by the mean values cited above and that the dK_M and dE_M uncertainty components of the equation would be specified by the cited standard deviation values.

Since only single M vs Z equations are presently available for the small-snow and ice-crystal categories (see Table 2), it is impossible to judge the dK_M and dE_M uncertainties that might exist between regression equations for the different types of small-snow, or the different types of ice crystals. About all that can be said, at the moment, is that the uncertainties will probably be as large, and perhaps larger, than those for large-snow.

We will now consider the component uncertainties, dZ_{rm} and dZ_s, of Eq. (59), which involve the reflectivity factor.

Reference is made to Table 4, where the $\overline{I}$, n_c, $\sigma_{\overline{P}_{r_1}}$, and Z values have been tabulated for the hydrometeor categories and radar conditions described in R No. 1 (in Tables B1 through B4). These same radar conditions are assumed to apply herein, as a starting point for estimating the dM uncertainties. Thus, except as noted in the footnote below, the uncertainty discussion of the present report is an extension of that of R No. 1.* Likewise, the uncertainty tables (Tables 4 and 6 herein) are extensions of Tables B1 and B2 of R No. 1.

The values of M (approximate values) listed in Table 4 were obtained from the tabulated Z values utilizing the relations

$$M = 0.0311\, Z^{.585}, \tag{60}$$

for rain, and

$$M = 0.00616\, Z^{.522}, \tag{61}$$

for large-snow. The constant, K_M, and exponent, E_M, values for these equations above are the mean values cited previously in this section.

With regard to the dZ_s uncertainties of the regression analyses, concerning the "scatter of the data values of Z about the regression line", reference is made to Figures 5, 6, and 7.

The first two figures show the M vs Z points and regression lines for two sets of disdrometer data (for rain) which were acquired during the Wallops storm of 22 March 1972. The standard errors of estimate (S.E.) for the two particular

*Uncertainty information about dZ_{rm} was presented in R No. 1 for two values of range-cell integration, $n_c = 1$ and $n_c = 8$. Just the $n_c = 8$ information is considered herein, since this was the number of range cells commonly included in the SAMS trajectory data acquired during the 1971-72 and 1972-73 seasons.

Table 4. Estimated Uncertainties of Liquid-Water-Content for Rain and Large-Snow Under Situation 1

Table 4. Estimated Uncertainties of Liquid-Water-Content for Rain and Large-Snow Under Situation 1

Hydrometeor Category	Assumed Radar Conditions (EHS-18 Radar)			Corresponding Values of		Uncertainty Contributions of Terms of Eq. (59)								Approx. Total Uncertainty (P. E. Summation)	
						First Term		Second Term		Third Term		Fourth Term			
	$\bar{L}$	n_c	$\sigma_{\bar{P}_{r_1}}$	Z	M	dZ_{rm}	Uncertainty Contribution to dM	dZ_s	Uncertainty Contribution to dM	Assumed dK_M	Uncertainty Contribution to dM	Assumed dL_M	Uncertainty Contribution to dM	dM	
	db		db	$mm^6 m^{-3}$	$gm\,m^{-3}$	$mm^6 m^{-3}$	$gm\,m^{-3}$	$mm^6 m^{-3}$	$gm\,m^{-3}$		$gm\,m^{-3}$		$gm\,m^{-3}$	$gm\,m^{-3}$	%
Rain	80	8	± 5	3092	0.341	± 2054	± 0.133	± 1400	± 0.0903	± 0.0017	± 0.0186	± 0.052	± 0.142	± 0.215	± 63.1
	80	8	± 10	3092	0.341	± 1562	± 0.101	± 1400	± 0.0903	± 0.0017	± 0.0186	± 0.052	± 0.142	± 0.197	± 57.9
	60	8	± 5	30.92	0.023	± 20.51	± 0.00892	± 14.00	± 0.00609	± 0.0017	± 0.00126	± 0.052	± 0.0041	± 0.0116	± 50.6
	60	8	± 10	30.92	0.023	± 15.62	± 0.00679	± 14.00	± 0.00609	± 0.0017	± 0.00126	± 0.052	± 0.0041	± 0.0101	± 43.9
Large-Snow	80	8	± 5	13,760	0.897	± 9136	± 0.311	± 18,000	± 0.613	± 0.0014	± 0.204	± 0.081	± 0.692	± 0.996	± 111
	80	8	± 10	13,760	0.897	± 6960	± 0.237	± 18,000	± 0.613	± 0.0014	± 0.204	± 0.081	± 0.692	± 0.976	± 109
	60	8	± 5	137.6	0.081	± 91.4	± 0.0281	± 180	± 0.0553	± 0.0014	± 0.0184	± 0.081	± 0.0323	± 0.0723	± 89.3
	60	8	± 10	137.6	0.081	± 69.6	± 0.0214	± 180	± 0.0553	± 0.0184	± 0.0184	± 0.081	± 0.0323	± 0.070	± 86.4

*Values are from Tables B1 and B2 of R No. 1.
**Values determined from Eqs. (60) and (61), as explained in text.

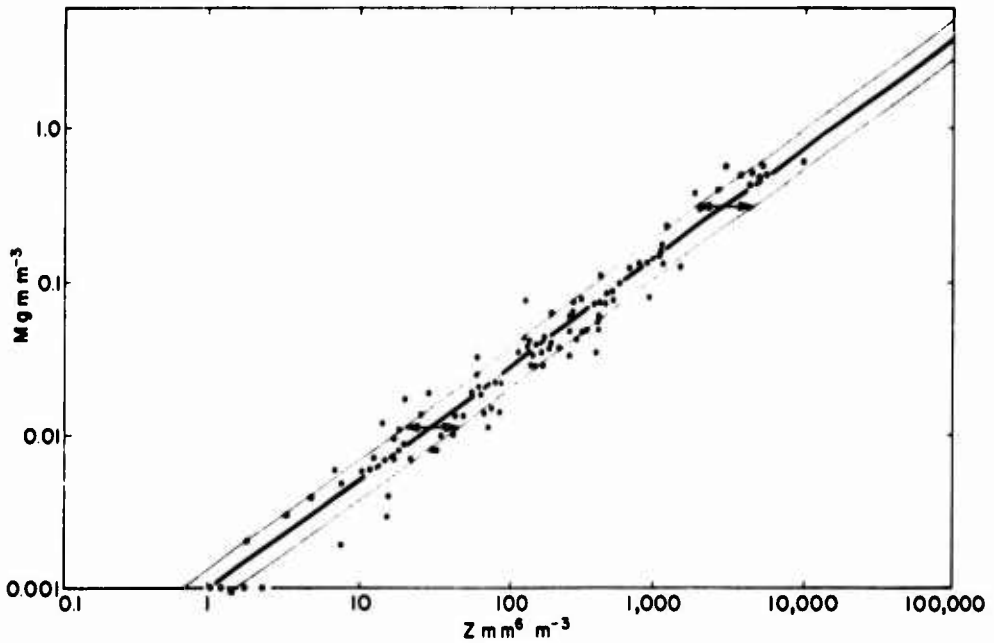

Figure 5. M vs Z Data for Rain, Obtained From Disdrometer A for the Wallops Storm of 22 March 1972. The regression line for the data is indicated and the thin, solid lines on either side show the bounds of the standard error of estimate. The arrows show the variation of Z about the two, particular Z values, 30.92 and 3092, which are listed and used in the uncertainty computations of Tables 4 and 5

Z values listed in Table 4 are illustrated in the figures by the horizontal arrows. The presented data are typical of disdrometer data obtained for the other storms of the 1971-72 season.

Figure 7 shows similar data for large-snow of dendritic-stellar type. The data are those of Ohtake and Henmi,[17] while additional computations and the regression analysis were performed by Vardiman.*

For the uncertainty estimations herein, it was assumed that the dZ_s values of Eq. (59), for the case of rain, would be given approximately by the "half difference" of the Z values indicated by the S.E. arrows of Figures 5 and 6. These dZ_s values are listed in Tables 4 and 5, under the section labeled "second term contributions".

The dZ_s values for large-snow were assumed to be given by the "half difference" of the Z values indicated by the S.E. arrows of Figure 7. These values are also listed in Tables 4 and 5.

*Unpublished work performed for AFCRL by L. Vardiman of Colorado State University (on reserve status from the Air Weather Service).

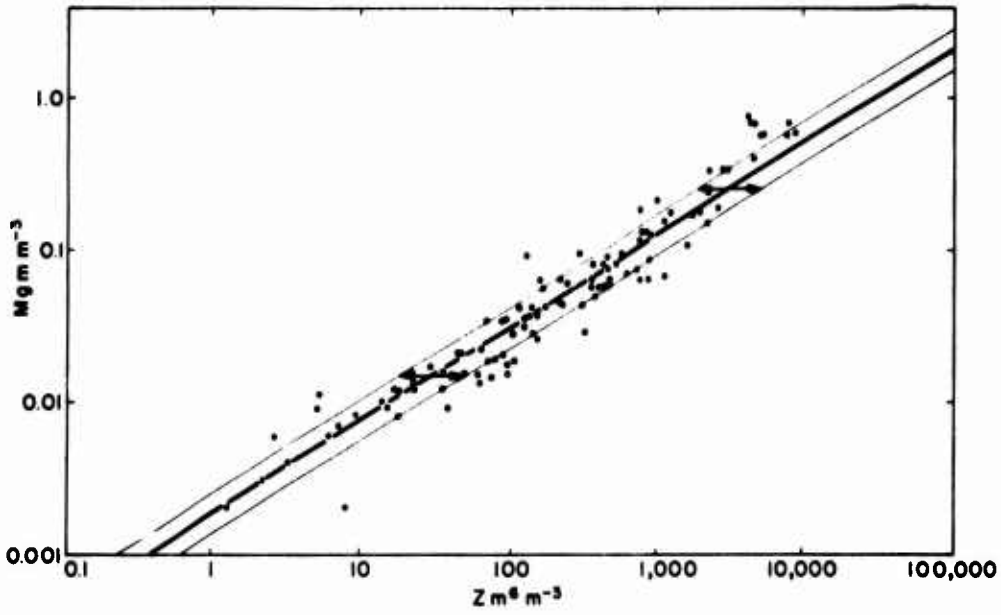

Figure 6. M vs Z Data for Rain, Obtained From Disdrometer B for the Wallops Storm of 22 March 1972. The regression line for the data is indicated and the thin, solid lines on either side show the bounds of the standard error of estimate. The arrows show the variation of Z about the Two, Particular Z Values, 30.92 and 3092, which are listed and used in the uncertainty computations of Tables 4 and 5.

The term contributions and total uncertainties of liquid-water-content are shown in Table 4 that were computed from Eq. (59) using the dK_M, dE_M, dZ_{rm}, and dZ_s estimates stated above. The dM (total) uncertainties listed in the next to the last column were obtained by probable error (P. E.) summation, that is,

$$dM = \sqrt{dM_1^2 + dM_2^2 + dM_3^2 + dM_4^2}\,, \tag{62}$$

of the separate term contributions, dM_1, dM_2, dM_3, and dM_4, of Eq. (59); see Eshbach,[59] for example, for a description of this type of summation.

The Table 4 results for the Situation 1 assumption reveal that the uncertainties of the liquid-water-content values along the SAMS missile trajectories range, in percentage terms, from about ±44 percent to ±111 percent.* The greatest

59. Eshbach, O. W. (1957) Handbook of Engineering Fundamentals, John Wiley and Sons, Inc., New York, N. Y., Sixth Printing

*Although it is convenient to cite percentage uncertainties for qualitative comparison purposes, it should be noted that large uncertainties, such as the above which are expressed in percent, are highly non-symmetric in their positive vs their negative values. For example, the positive value can exceed 100 whereas the negative value cannot. The meaningful uncertainty values of Table 4, also of Table 5, are the dM values of the next to the last columns.

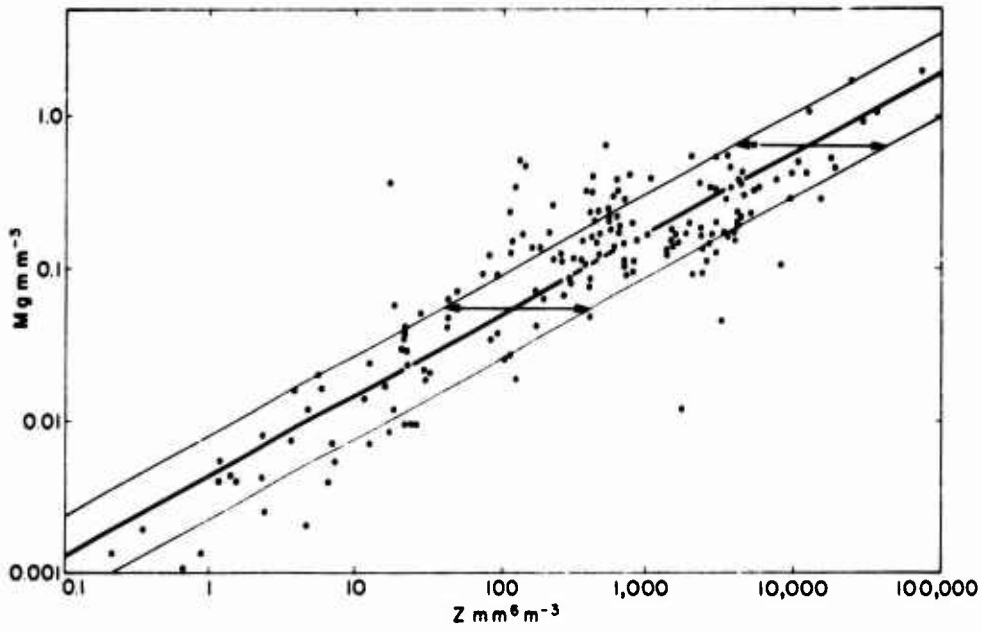

Figure 7. M Vs Z Data of Ohtake* for Large-Snow of Dendritic-Stellar Type. The regression line for the data is indicated and the thin, solid lines on either side show the bounds of the standard error of estimate. The arrows show the variation of Z about the two, particular Z values, 137.6 and 13,760, which are listed and used in the uncertainty computations of Tables 4 and 5

uncertainties occur for large-snow having large liquid-water-content; the smallest occur with rain having small liquid-water-content.

6.2 Estimated Uncertainties of Liquid-Water-Content for Rain and Large-Snow Under Situation 2

If quantitative surface and aircraft measurements exist specifying the size-distribution properties of the storm hydrometeors (and supplementing the radar measurements, which is the Situation 2 presumption), these data, appropriately analyzed, provide information about the specific regression equations of M vs Z that pertain to each hydrometeor type observed in the storm.

In this situation, since there is no doubt as to which regression equation applies, the dK_M and dE_M uncertainty components of Eq. (59) have zero values and the equation reduces to

$$dM = \frac{K_M E_M Z^{E_M}}{Z} \left(dZ_{rm} + dZ_s \right). \tag{63}$$

*Unpublished data, see footnote on p. 50.

Table 5. Estimated Uncertainties of Liquid-Water-Content for Rain and Large-Snow Under Situation 2

Table 5. Estimated Uncertainties of Liquid-Water-Content for Rain and Large-Snow Under Situation 2

Hydrometeor Category	Assumed Radar Conditions* (FPS-18 Radar) $\bar{I}$ db	n_c	$\sigma_{\bar{P}_{r_1}}$ db	Corresponding Values of Z* $mm^6 m^{-3}$	M** $gm\,m^{-3}$	Uncertainty Contributions of Terms of Equation: First Term dZ_r^* $mm^6 m^{-3}$	First Term: Uncertainty Contribution to dM $gm\,m^{-3}$	Second Term dZ_s $mm^6 m^{-3}$	Second Term: Uncertainty Contribution to dM $gm\,m^{-3}$	Approx. Total Uncertainty (P. E. Summation) dM $gm\,m^{-3}$	%
Rain	80	8	± 5	3092	0.341	± 2054	± 0.133	± 1400	± 0.0903	± 0.160	± 47.0
	80	8	± 10	3092	0.341	± 1562	± 0.101	± 1400	± 0.0903	± 0.135	± 39.7
	60	8	± 5	30.92	0.023	± 20.51	± 0.00892	± 14	± 0.00609	± 0.0108	± 47.0
	60	8	± 10	30.92	0.023	± 15.62	± 0.00679	± 14	± 0.00609	± 0.00913	± 39.7
Large-Snow	80	8	± 5	13,760	0.897	± 9136	± 0.311	± 18,000	± 0.613	± 0.687	± 76.6
	80	8	± 10	13,760	0.897	± 6960	± 0.237	± 18,000	± 0.613	± 0.657	± 73.2
	60	8	± 5	137.6	0.081	± 91.4	± 0.0281	± 180	± 0.0553	± 0.0620	± 76.6
	60	8	± 10	137.6	0.081	± 69.6	± 0.214	± 180	± 0.0553	± 0.0593	± 73.2

*Values are from Tables B1 and B2 of R No. 1.
**Values determined from Eqs. (60) and (61), as explained in text.

For the same assumptions about dZ_{rm} and dZ_s that were stated previously, the term contribution and total uncertainties of liquid-water-content are shown in Table 5 which were computed from Eq. (60). Probable-error summation of the term contributions was used to obtain the dM values, as in the case of the Table 4 computations.

A comparison of the dM values of Tables 4 and 5 reveals that, when disdrometer data are available to supplement the SAMS radar measurements, the uncertainties of the trajectory values of liquid-water-content in the rain region of the storm are reduced by about ±4 percent to ±16 percent, relative to the uncertainties of the radar measurements alone. The accuracy of measurement, in other words, is improved by these amounts. Similarly, when aircraft data are acquired to supplement the radar measurements, the accuracy of the liquid-water-content values in the large-snow region of the storms is improved by some ±13 percent to ±34 percent, relative to the uncertainties of the radar measurements alone. The accuracy enhancement to be anticipated from the acquisition of aircraft data in the small-snow and ice-crystal regions of the storm is probably as large, or larger, than these last cited values.

6.3 Comments

Two comments are pertinent concerning the Table 4 and Table 5 results.

It must be emphasized, first, as was also emphasized in R No. 1, that the table values are merely, first, gross estimates of the possible uncertainty values. Additional, better data must be acquired and more-careful analyses performed to establish the definitive values of the uncertainties.

Second, it should be noted that an a-priori assumption was made, under the Situation 1 hypothesis (of radar measurements only), that knowledge existed concerning the general category of hydrometeors that were producing radar echo, whether they were rain, large-snow, small-snow, or ice crystals. In actual fact, it is impossible, by radar means alone, to differentiate the latter three categories of ice hydrometeors which may be present at storm altitudes above the melting level. Aircraft measurements are required to do this. The point here, which is an important point that could not be verbalized previously, is that the true uncertainties of the liquid-water-content values, as assessed from radar measurements only, for storm altitudes above the melting level, may be substantially larger than the single category, large-snow uncertainties shown in Table 4. The dK_M and dE_M component-uncertainties that enter Eq. (59) will actually be larger than the Table 4 estimates when aircraft information is lacking, because even the hydrometeor categories themselves cannot then be identified (the dK_M and dE_M uncertainties would reflect the larger "category differences" of Table 2, rather

than the "type differences" within the category). The uncertainties of liquid-water-content would be correspondingly increased, in such case, conceivably by as much as a factor of two, dependent upon the particular storm conditions.

These larger, possible uncertainties are mentioned because some of the SAMS storm data obtained during the 1970-73 seasons consisted essentially of "radar measurements only". This would include situations in which aircraft data could not be acquired that were representative of the hydrometeor conditions along the missile trajectory at firing time as, for example, in the case of missiles launched into convective-type storms having appreciable spatial-temporal variability.

6.4 Uncertainties of the Integral of Liquid-Water-Content

The dM uncertainties discussed above are the uncertainties that pertain to single-point measurements along the missile trajectory which have been spatially averaged over the volumetric extent of the radar-integration-volume and time averaged throughout the duration of the integration period [see Eqs. (A3) and (A4) of R No. 1]. Additional spatial averaging is performed when the radar data are processed by computer, as was the case with the SAMS data of the 1972-73 season.

The cloud-physics parameter of primary concern to the SAMS ABRES program is the integral of liquid-water-content along segment portions of the missile trajectory which correspond, in length extent, to the resolution distance of the erosion information that is telemetered to the ground from the sensors aboard the missile. Detailed correlations of erosion parameters vs cloud physics parameters must necessarily be concerned with a "matching correspondence" of the "length resolution" of the separate parameters.

Thus, it is the path integral of liquid-water-content at particular resolution distances which is the parameter of final cloud-physics interest to SAMS; and the "accuracy level" of the AFCRL measurements performed for SAMS is directly related to the uncertainties involving this integral. These uncertainties should never exceed the value-estimates discussed in the preceding sections, which pertain to single-point measurements of M. Rather, the uncertainties will be smaller, in degree dependent on the nature and details of such things as the radar integration, the computer averaging, the erosion instrumentation of the missile, and the analysis methods that were employed in the particular Wallops storms of prior SAMS investigation. The geometry of the radar scan pattern and sampling volume relative to that of the missile trajectory also enters the problem.

These matters should be investigated, if definitive information regarding uncertainties is desired. It is beyond the scope of the present report, however, to attempt such consideration.

7. SIZE-DISTRIBUTION INFORMATION FOR THE DIFFERENT HYDROMETEOR TYPES

The nature and amount of the nose-tip erosion experienced by the SAMS missiles are influenced by the types and size-distribution properties of the hydrometeors along the missile trajectories. This information, as mentioned previously, is acquired by aircraft measurements.

Since the aircraft measurements are made subsequent to the launch times of the missiles and in spatially different parts of the storms than those penetrated by the missiles, the size-distribution information obtained is not specifically applicable to the missile trajectories. It is merely representative of the general storm conditions during the time period following the missile firing.

The size-distribution analyses that have been performed on the aircraft data for the SAMS storms to date have been relatively few. There were various instrumentation failures during the aircraft flights, with consequent loss of data. This limited the available samples. Also, the analyses are painstaking and time-consuming; hence the samples must be selected with care and be limited in number. (These results will be presented in the forthcoming data reports of the series.)

In view of these problems of the non-specificity and limited number of the aircraft samples for the past storms and for purposes of erosion assessment, there is a need for a method of estimating the approximate size distribution properties of the hydrometeors along the missile trajectories. One such method will be described in this section which concerns rain drops, snow aggregates, and ice crystals of precipitation size (>80 microns, approximately). Methods for estimating the size spectra of water droplets of cloud size (<80 microns) will be discussed later in future reports.

Laws and Parsons,[5] Wexler,[2] and Marshall and Palmer,[4] as mentioned in Section 3.1, demonstrated that the variation of the number concentration of raindrops with diameter, D, could be specified approximately by a distribution function of exponential type,

$$N = N_o e^{-\Lambda D} . \tag{64}$$

From the data of Marshall et al,[3] Marshall and Palmer[4] demonstrated that N_o had the value 8000 (m^{-3} mm^{-1}) and that Λ was functionally dependent on the precipitation rate, P (in mm hr^{-1}), as

$$\Lambda = 4.1\, P^{-0.21} \ mm^{-1} . \tag{65}$$

Gunn and Marshall[14] used this same distribution function to describe the size-distribution properties of aggregate snow particles. The diameter D was

replaced by the equivalent-melted-diameter and they ascertained from their data analyses that

$$N_o = 3.8 \times 10^3 \; P^{-.87} \; m^{-3} \; mm^{-1} , \tag{66}$$

and

$$\Lambda = 2.55 \; P^{-.48} \; mm^{-1} . \tag{67}$$

Other investigators have used the distribution function of Eq. (64) in conjunction with various data-dependent assumptions about the equations for N_o and Λ. Certain of these investigators are identified in Table 6 and their particular equations are listed.

Table 6. The Equations (Data Supported) of Various Investigators Regarding the N_o and Λ Terms of the Exponential Distribution Function, Eq. (64) Herein

Investigators	Precipitation Category	Equations for N_o m^{-3} mm^{-1}	Equations for Λ mm^{-1}
Marshall and Palmer[4]	Continuous Rain	$N_o = 8{,}000$	$\Lambda = 4.1 \; P^{-.21}$
Joss et al[40]	Drizzle	$N_o = 30{,}000$	$\Lambda = 5.7 \; P^{-.21}$
	Widespread, Continuous Rain	$N_o = 7{,}000$	$\Lambda = 4.1 \; P^{-.21}$
	Thunderstorm, Rain	$N_o = 1{,}400$	$\Lambda = 3.0 \; P^{-.21}$
Sekhon and Srivastava[30]	Thunderstorm, Rain	$N_o = 7{,}000 \; P^{.37}$	$\Lambda = 3.8 \; P^{-.14}$
Ramana Murty and Gupta (1959)	Monsoon Rain, Orographic	$N_o = 7{,}500 \; P^{-.25}$	$\Lambda = 0.81 \; P^{.27}$
	Monsoon Rain, Non-Orographic	$N_o = 1{,}500 \; P^{.23}$	$\Lambda = 1.14 \; P^{.17}$
Gunn and Marshall[14]	Aggregate Snow	$N_o = 3{,}800 \; P^{-.87}$	$\Lambda = 2.55 \; P^{-.48}$
Sekhon and Srivastava[23]	Aggregate Snow	$N_o = 2{,}500 \; P^{-.94}$	$\Lambda = 2.29 \; P^{-.45}$

In the development herein, we will depart somewhat from the work of these previous investigators. We will use the distribution function of Eq. (64), but will obtain expressions for N_o and Λ that are written in terms of the liquid-water-content, rather than P. In essence, we will follow the development of Sekhon

and Srivastava.[30] Additionally, however, we will develop equations which are consistent with the M vs Z relationships of Table 2.*

The liquid-water-content of the drops or particles specified by Eq. (64) for all diameters (or equivalent melted diameters) of the drops or particles, from D = 0 to D = ∞, is given by

$$M = \frac{\pi}{6} \times 10^{-3} \rho_w \int_0^\infty N D^3 dD = \frac{\pi}{6} \times 10^{-3} \rho_w N_o \int_0^\infty e^{-\Lambda D} D^3 dD , \quad (68)$$

where ρ_w is the density of water, in gm cm^{-3}, and M is given in gm m^{-3}. On integration, this equation becomes

$$M = \frac{\pi}{6} \times 10^{-3} \frac{\rho_w N_o \Gamma(4)}{\Lambda^4} , \quad (69)$$

where $\Gamma(4)$ is the gamma function of 4.

The radar reflectivity-factor for the distribution of drops or particles described by Eq. (64) is, for all diameters from D = 0 to D = ∞,

$$Z = \int_0^\infty N D^6 dD = N_o \int_0^\infty e^{-\Lambda D} D^6 dD , \quad (70)$$

which, integrated, yields

$$Z = \frac{N_o \Gamma(7)}{\Lambda^7} \ mm^6 \ m^{-3} , \quad (71)$$

where $\Gamma(7)$ is the gamma function of 7.

The parameter Λ can be eliminated between Eqs. (69) and (71) to obtain

$$N_o = \frac{6 \times 10^3 M}{\pi \Gamma(4) \rho_w} \left[\frac{6 \times 10^3 \Gamma(7) M}{\pi \rho_w \Gamma(4) Z} \right]^{4/3} , \quad (72)$$

which, from knowledge that $\rho_w = 1.0$, $\Gamma(4) = 6$, and $\Gamma(7) = 720$, reduces to

$$N_o = 4.46 \times 10^9 M \left(\frac{M}{Z} \right)^{4/3} \ m^{-3} \ mm^{-1} . \quad (73)$$

Alternately, N_o can be eliminated between Eqs. (69) and (71) with the result, after evaluation of ρ_w, $\Gamma(4)$ and $\Gamma(7)$,

*In practice, for practical equation accuracy, integration to D = ∞ implies integration to some maximum diameter approximately ≥ 15/Λ.

$$\Lambda = 61.2\left(\frac{M}{Z}\right)^{1/3} \text{ mm}^{-1}. \tag{74}$$

The empirical equations relating M and Z were discussed in Section 4.2. It was pointed out that the equations are of the form

$$M = K_M Z^{E_M}, \tag{75}$$

and that the particular values of K_M and E_M for each hydrometeor category (rain, large-snow, small-snow, and ice crystals) and type were obtained from regression analyses performed on data pertaining to the individual types. The values used in the SAMS program were listed in Table 2.

When Eq. (75) is substituted into Eq. (73) first, and into Eq. (74) second, we obtain

$$N_o = 4.46 \times 10^9 \; K_M^{\frac{4}{3E_M}} \; M^{\frac{7E_M - 4}{3E_M}} \text{ m}^{-3} \text{ mm}^{-1} \tag{76}$$

and

$$\Lambda = 61.2 \; K_M^{\frac{1}{3E_M}} \; M^{\frac{E_M - 1}{3E_M}} \text{ mm}^{-1}, \tag{77}$$

which permit the specification of the N_o and Λ values for each hydrometeor type (from knowledge of K_M and E_M) as functions of the liquid-water-content. These equations, for the hydrometeor types defined for the SAMS program, are listed in Table 7.*

The N_o and Λ equations of this table, when substituted into the distribution function of Eq. (64), provide approximate information about how the number concentration of the hydrometeors varies with the drop or particle diameter (equivalent-melted-diameter) for any given value of liquid-water-content. Information is also provided about the distribution of liquid-water-content within the population, by diameter size. This distribution function, which is the third moment of the function for number concentration, is

$$M_D = \frac{\pi}{6} \times 10^{-3} \rho_w N_o e^{-\Lambda D} D^3 \text{ gm m}^{-3} \text{ mm}^{-1}. \tag{78}$$

*The equations are also shown in Table 8, written in terms of the precipitation rate, P (accomplished by use of the P vs M relationships of Table 3). These transformed equations permit direct comparisons with the equations of the other investigators shown in Table 6.

Table 7. The Equations for N_O, Λ, and N_T for the AFCRL Hydrometeor Types Defined for SAMS, Written in Terms of the Liquid-Water-Content [See Table 2 and Eqs. (76), (77), and (80) of the text]

Hydrometeor Region and Type	Symbol	Values of		Equations for		
		K_M	E_M	N_O $m^{-3}\ mm^{-1}$	Λ mm^{-1}	N_T m^{-3}
Ice Crystal Region						
Columns, Bullets, Rosettes	C_1	0.038	0.529	$N_O = 1,180,000\ M^{-.187}$	$\Lambda = 7.80\ M^{-.297}$	$N_T = 151,000\ M^{.110}$
Small-Snow Region						
Single-Crystal Snow	SS_S	0.0145	0.538	$N_O = 124,000\ M^{-.145}$	$\Lambda = 4.44\ M^{-.286}$	$N_T = 27,900\ M^{.141}$
Large-Snow Region						
Large Aggregates of Columns, Bullets	LS_1	0.00672	0.615	$N_O = 87,000\ M^{.165}$	$\Lambda = 5.07\ M^{-.209}$	$N_T = 21,400\ M^{.374}$
Large Aggregates of Needles	LS_2	0.00686	0.477	$N_O = 4,000\ M^{-.462}$	$\Lambda = 1.88\ M^{-.365}$	$N_T = 2,120\ M^{-.096}$
Large Aggregates of Plates	LS_3	0.00495	0.596	$N_O = 31,100\ M^{.096}$	$\Lambda = 3.14\ M^{-.226}$	$N_T = 9,880\ M^{.322}$
Large Aggregates of Grauple, Pellets	LS_4	0.00807	0.394	$N_O = 368\ M^{-1.051}$	$\Lambda = 1.04\ M^{-.513}$	$N_T = 355\ M^{-.538}$
Large Aggregates of Dendrites, Stellars	LS_5	0.00420	0.526	$N_O = 4,220\ M^{-.202}$	$\Lambda = 1.91\ N^{-.300}$	$N_T = 2,210\ M^{.099}$
Cunningham Snow *	LS_C	0.01340	0.385	$N_O = 1,460\ M^{-1.130}$	$\Lambda = 1.46\ M^{-.532}$	$N_T = 996\ M^{-.597}$
Rain Region						
Disdrometer Data, 3 February 1972	R_D	0.00146	0.635	$N_O = 4,960\ M^{.234}$	$\Lambda = 1.99\ N^{-.192}$	$N_T = 2,500\ M^{.425}$
Disdrometer Data, 17 February 1972	R_D	0.00419	0.490	$N_O = 1,510\ M^{-.388}$	$\Lambda = 1.42\ M^{-.347}$	$N_T = 1,020\ M^{-.041}$
Disdrometer Data, 17 March 1972	R_D	0.00376	0.571	$N_O = 9,720\ M^{-.002}$	$\Lambda = 2.35\ M^{-.250}$	$N_T = 4,130\ M^{.249}$
Disdrometer Data, 22 March 1972	R_D	0.00134	0.667	$N_O = 8,070\ M^{.334}$	$\Lambda = 2.24\ M^{-.166}$	$N_T = 3,600\ M^{.501}$

*This type of snow was defined and used only during the 1971-72 SAMS season.

Table 8. The Equations for N_o, Λ, and N_T for the AFCRL Hydrometeor Types Defined for SAMS, Written in Terms of the Precipitation Rate, Which Permits Comparisons With the Equations of Table 6. The equations listed were derived from the Table 7 equations using the M vs P relations listed in Table 2

Hydrometeor Region and Type	Symbol	Equations for		
		N_o $m^{-3}\ mm^{-1}$	Λ mm^{-1}	N_T m^{-3}
Ice Crystal Region				
Columns, Bullets, Rosettes	C_1	$N_o = 1,580,000\ P^{-.138}$	$\Lambda = 12.5\ P^{-.218}$	$N_T = 127,000\ P^{.081}$
Small-Snow Region				
Single-Crystal Snow	SS_S	$N_o = 151,000\ P^{-.125}$	$\Lambda = 6.60\ P^{-.246}$	$N_T = 22,900\ P^{.121}$
Large-Snow Region				
Large Aggregates of Columns, Bullets	LS_1	$N_o = 69,200\ P^{.156}$	$\Lambda = 5.43\ P^{-.196}$	$N_T = 12,700\ P^{.352}$
Large Aggregates of Needles	LS_2	$N_o = 8,240\ P^{-.403}$	$\Lambda = 3.34\ P^{-.319}$	$N_T = 2,470\ P^{-.084}$
Large Aggregates of Plates	LS_3	$N_o = 27,000\ P^{.091}$	$\Lambda = 4.37\ P^{-.213}$	$N_T = 6,180\ P^{.304}$
Large Aggregates of Grauple, Pellets	LS_4	$N_o = 2,980\ P^{-.846}$	$\Lambda = 2.87\ P^{-.413}$	$N_T = 1,040\ P^{-.433}$
Large Aggregates of Dendrites, Stellars	LS_5	$N_o = 5,280\ P^{-.183}$	$\Lambda = 2.67\ P^{-.272}$	$N_T = 1,980\ P^{.090}$
Cunningham Snow*	LS_C	$N_o = 6,850\ P^{-.957}$	$\Lambda = 3.03\ P^{-.451}$	$N_T = 2,260\ P^{-.506}$
Rain Region				
Disdrometer Data, 3 February 1972	R_D	$N_o = 2,530\ P^{.213}$	$\Lambda = 3.45\ P^{-.174}$	$N_T = 734\ P^{.387}$
Disdrometer Data, 17 February 1972	R_D	$N_o = 4,330\ P^{-.310}$	$\Lambda = 3.78\ P^{-.278}$	$N_T = 1,140\ P^{-.033}$
Disdrometer Data, 17 March 1972	R_D	$N_o = 9,760\ P^{-.001}$	$\Lambda = 4.50\ P^{-.212}$	$N_T = 2,170\ P^{.210}$
Disdrometer Data, 22 March 1972	R_D	$N_o = 3,140\ P^{.304}$	$\Lambda = 3.59\ P^{-.151}$	$N_T = 875\ P^{.455}$

*This type of snow was defined and used only during the 1971-72 season.

The N_o and Λ terms of this equation are likewise specified, for each hydrometeor type, by reference to Table 7. The independent variable of the above equation is D; the other parameters on the right are constants for any given value of total liquid-water-content.

The values of the radar reflectivity factor for the population (the values per diameter bandwidth) are distributed according to the sixth moment of the function for number concentration, or as

$$Z_D = N_o e^{-\Lambda D} D^6 \quad mm^6\ m^{-3}\ mm^{-1} . \tag{79}$$

Other characteristic or useful parameters of the distributions can be specified analytically. For example, the total number concentration of the drops or particles, of all sizes within the populations, is given by

$$N_T = 7.29 \times 10^7 \; K_M^{\frac{1}{E_M}} \; M^{\frac{2E_M - 1}{E_M}} \quad m^{-3} , \tag{80}$$

[from integration of Eq. (64) and substitutions from Eqs. (76) and (77)]. The K_M and E_M values for the particular hydrometeor types are listed in Table 7 (also in Table 2).

The "median volume diameter" of the distribution function for liquid-water-content is a parameter of common, conventional reference. This diameter, first derived by Atlas[60] is,

$$D_o = 3.67/\Lambda \quad mm . \tag{81}$$

The "modal diameters" of the M_D and Z_D distributions are also characteristic parameters of interest. These diameters, which specify the peak-value points of the bandwidth values of liquid-water-content and reflectivity factor are given respectively by

$$D' = 3/\Lambda \quad mm \tag{82}$$

and

$$D'_z = 6/\Lambda \quad mm . \tag{83}$$

These expressions were derived by differentiating Eqs. (78) and (79) and determining the diameter values corresponding to maximum M_D and Z_D.

60. Atlas, D. (1953) Optical extinction by rainfall, J. Meteorol. 10:486-488.

Each of the above Eqs. (64) and (78) through (82), can be evaluated for any given point along the SAMS missile trajectories. The hydrometeor regions of the storms and the hydrometeor types within regions are established by aircraft observation, as discussed earlier and as is illustrated in Figures 3 and 4. This information, by reference to Table 7, permits the determination of the N_o and Λ equations for the given hydrometeor type, which in turn permits the specification of the distribution functions of Eqs. (64), (78), and (79). These equations, also Eqs. (80) through (83), can then be evaluated for the particular liquid-water-content value that pertains to the selected trajectory point.

A specific example may be helpful.

Consider the profile plot of liquid-water-content of Figure 4, for the SAMS missile flight of 2 February 1973. Consider a point on this profile which lies within the "large-snow region" of the storm and is located at a trajectory altitude of 3.8 km. The liquid-water-content value at this altitude is 0.3 gm m^{-3} (by convenient choice).

The large-snow on this day was determined to be of the type called "aggregates of plates". The N_o and Λ equations for this hydrometeor type are as shown in Table 7. These equations, when substituted in Eqs. (64), (78), and (79) provide the particular distribution functions,

$$N = 27{,}700\ e^{-4.12\,D} \qquad m^{-3}\,mm^{-1}, \tag{84}$$

for number concentration,

$$M_D = 14.5\ e^{-4.12\,D}\ D^3 \qquad gm\ m^{-3}\,mm^{-1}, \tag{85}$$

for liquid-water-content, and

$$Z_D = 27{,}700\ e^{-4.12\,D}\ D^6 \qquad mm^6\ m^{-3}\,mm^{-1}, \tag{86}$$

for the radar reflectivity factor.

Plots of these equations are presented in Figure 8, to illustrate their characteristics. The upper plot shows the size distribution of the number concentration of the snow aggregates. The total number of the aggregates within the population, N_T, is indicated. The plot in the middle shows the distribution of the liquid-water-content; the plot at the bottom shows the distribution of the radar reflectivity factor. The integrated total value of the radar reflectivity factor for the trajectory point was 990 $mm^6\ m^{-3}$, which value is consistent with the M vs Z equation of Table 2, for large-snow, of type LS_3.

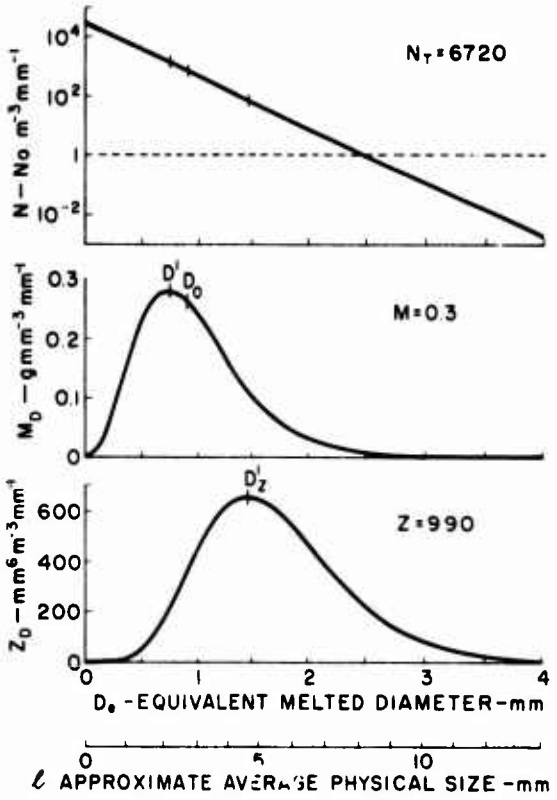

Figure 8. Plots Illustrating the Type of Size-Spectrum Information That Can Be Obtained From the Non-Truncated Distribution Functions (Discussed in the Text) When They Are Applied to Any Given Altitude Point Along the SAMS Missile Trajectories, Excluding Points Located Within the Melting Zone

The median-volume-diameter of the population, D_0 [see Eq. (81)], is indicated on the middle plot; the modal diameters, D' and D'_z [see Eqs. (82) and (83)], are indicated on the middle and bottom plots. Two abscissa scales are shown. The upper one indicates the equivalent melted diameters of the snow aggregates; the lower one indicates the approximate average physical dimensions of the particles [see Eq. (89) for the scale relationship assumed].

The total number of snow particles of all sizes in this population example is N_T = 6720 from Eq. (80) and the K_M and E_M values of Table 7. The median and modal diameters of the M_D distribution are D_0 = 0.89 mm (equivalent melted

diameter) and $D' = 0.73$ mm from Eqs. (81) and (82). The modal diameter of the Z_D distribution is $D_z' = 1.46$ mm from Eq. (83). These diameters are indicated in the Figure 8 diagrams.

This example demonstrates the type of size-distribution information that can be established for any trajectory point of the Figure 4 profile that is located within one of the four (possible) hydrometeor regions specified herein. Similar information can also be established for two of the three transition zones, the exception being the melting zone. The K_M and E_M values within the zones above the melting level can be interpolated with altitude above the zone bases, as discussed in Sections 4.5 and 4.6. The N_o and Λ equations for any given height within the zones can then be determined by direct evaluation of Eqs. (76) and (77), which permits the specification of the distribution functions of Eqs. (64), (78), and (79); also of the auxiliary Eqs. (80) through (83).

Distribution function and totals information is provided in Figures 9 through 17 for all of the hydrometeor types observed in the storms of the 1971-73 SAMS seasons. The upper diagrams show the distribution of the number concentration of the drops or particles for three different values of liquid-water-content, which are indicated. The middle diagrams show the distribution of liquid-water-content with the equivalent-melted-diameter of the drops or particles, and the bottom diagrams show the distribution of the radar reflectivity factor. The total numbers of the drops or particles in the distributions, N_T, are listed, as are the total Z values. The median-volume-diameter points of the distributions [the D_o points, see Eq. (81)] are shown by the large black dots. Two abscissa scales have been drawn for the figures pertaining to ice hydrometeors. The upper scale shows the equivalent melted diameters of the particles; the lower scale indicates the approximate physical dimensions (average dimensions) of the particles. The scale equations relating the physical length, ℓ, to the equivalent melted diameter, D_e, are the following:

$$D_e = 0.44\, \ell^{0.84}, \tag{87}$$

for ice crystals, type C_1, (see Table 2 for type identification)

$$D_e = 0.324\, \ell^{0.805}, \tag{88}$$

for small-snow, type SS_S, and

$$D_e = 0.40\, \ell^{0.875}, \tag{89}$$

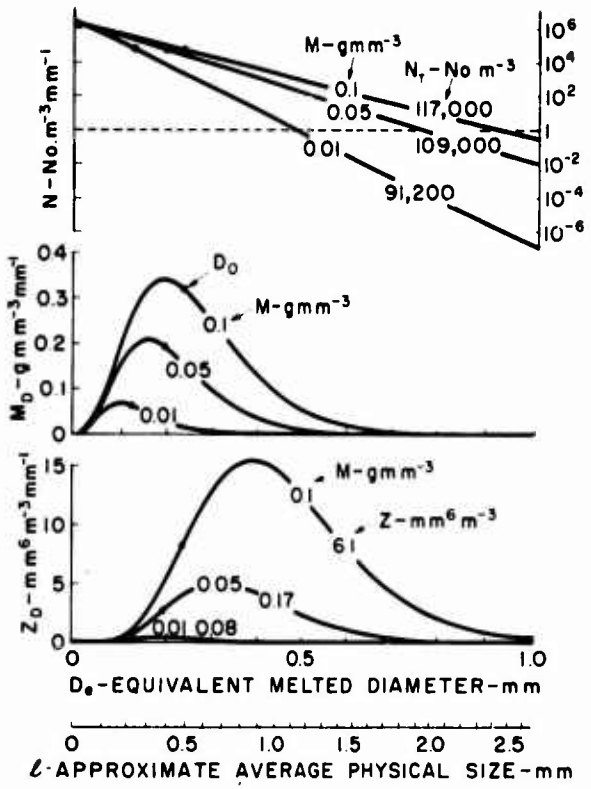

Figure 9. Distribution-Function Plots for Type C_1 Ice-Crystals for Three Different Values of Liquid-Water-Content. The plots of the upper diagram show the size distribution of the number concentration of the ice-crystals for liquid-water-content values of 0.01, 0.05, and 0.1 gm m^{-3}. The number total, N_T, of the ice crystals within the populations is also indicated. The plots of the middle diagram show the distribution of the liquid-water-content by crystal size for the same values of total liquid-water-content as cited above. The median-volume-diameters, D_0, are indicated by the large black dots. These diameter points are also shown in the other distributions as well. The plots of the bottom diagram show the size spectra of the radar reflectivity factor. The total integrated values of the radar reflectivity factor are additionally shown. Two abscissa scales have been drafted on the figure. The upper scale shows the equivalent melted diameters of the ice-crystals; the lower scale provides approximate information about the average physical sizes of the crystals. The scale relationship is specified by Eq. (87)

for large-snow, type LS_5. The latter equation pertains strictly to the large-snow type LS_5, but was used for the type LS_C of Figure 11, and the type LS_3, of Figure 12, in lieu of other knowledge. The equations were developed by Cunningham from literature information and empirical data.

The distribution plots of Figures 9 through 17 will serve to inform the reader of the general nature of the size distribution characteristics and differences that exist among the different hydrometeor types that have been discussed in this report.

Several comments are pertinent before concluding this section.

It should be noted that the size-distribution information provided by the techniques and equations described herein is only a first, gross approximation.

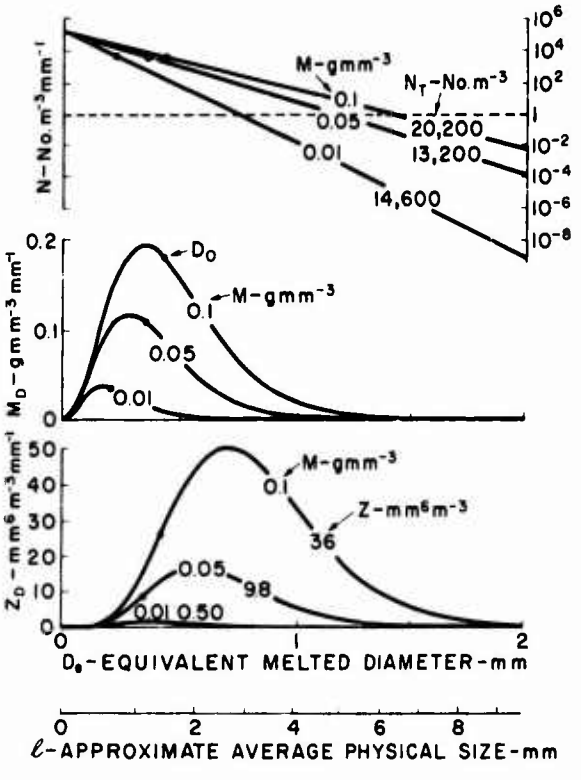

Figure 10. Distribution-Function Plots for Small-Snow, Type SS_S, for Three Different Values of Liquid-Water-Content. The plots are similar to those described in the Figure 9 caption. Note that the scale of equivalent melted diameter extends to 2 mm, which differs from the Figure 9 scale

There are two major reasons for this. First, the actual hydrometeors in the Wallops storms are not necessarily size-distributed in an exponential manner. Observed distributions reveal substantial individual-sample-departures from exponentiality, although, on the average, any large number of samples will reveal distinct tendencies toward exponentiality. Second, in the development herein, which follows the more or less conventional treatments of the past, the distribution function of Eq. (64) is integrated between D = 0 and D = ∞.* This is physically unrealistic, of course, since drops or particles of zero size do not exist,

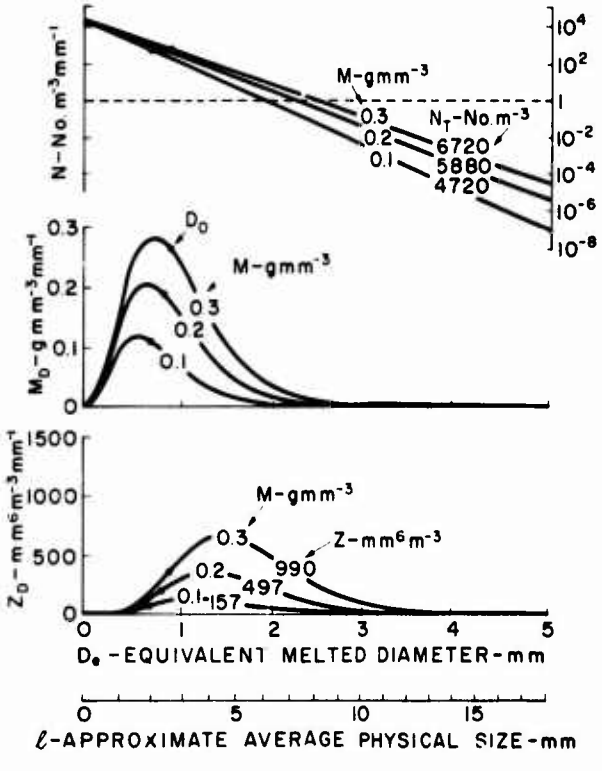

Figure 11. Distribution-Function Plots for Large-Snow, Type LS_3, for Three Different Values of Liquid-Water-Content. The plots are similar to those described in the Figure 9 caption. Note that the liquid-water-content values are 0.1, 0.2, and 0.3; also that the scale of equivalent melted diameter extends to 5 mm

*It can be shown that, for practical purposes, integration to $D = \infty$ is equivalent to integrating to a maximum diameter defined by $D_m \geq 15/\Lambda$, or [see Eq. (82)] $D_m \geq 5D'$.

and since there is also an upper diameter limit of the sizes of the largest drops or particles. The distributions are obviously truncated at some minimum diameter value, also at some maximum diameter value. In addition to this physical truncation of the hydrometeor populations, truncation can also occur instrumentally, since any given aircraft instrument may be incapable of sensing drops or particles smaller than a particular minimum size, or larger than some particular maximum size. These truncation problems, which are of vital concern to SAMS, are currently being considered at AFCRL. A double truncation model has been developed which extends and simplifies certain of the equations of Sekhon and Srivastava[30] and particularizes them for SAMS application. This model will be described and illustrated later in the report series.

The following statements may be made about the physical deficiencies of the non-truncated equations presented in this section and illustrated in Figures 8 through 17. For any given hydrometeor type and liquid water content, the

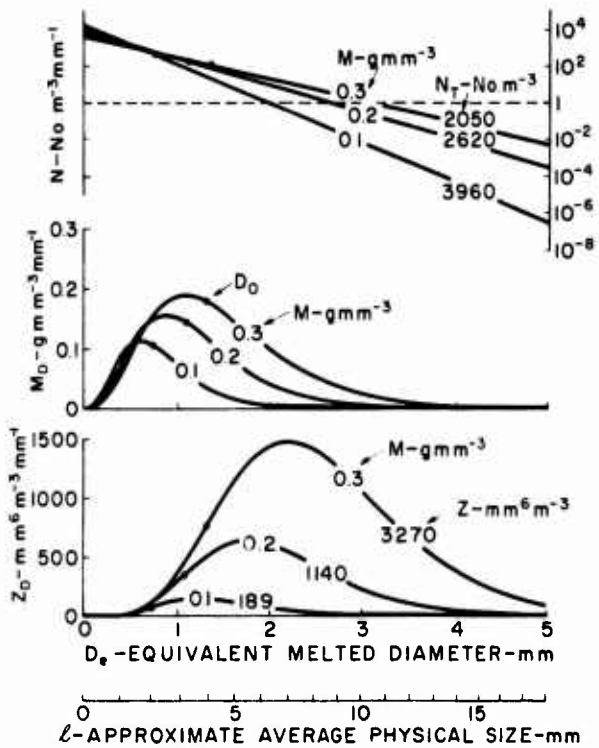

Figure 12. Distribution-Function Plots for Large-Snow, Type LS_C, for Three Different Values of Liquid-Water-Content. The plot scaling and liquid-water-content values plotted are identical to Figure 11

non-truncated equations (compared to the more realistic truncated equations) will tend to (1) overestimate the values of Λ, (2) overestimate the values of N_o, (3) overestimate the number of the smallest drops or particles, (4) underestimate the number of the largest drops or particles, and (5) overestimate the total number of the drops or particles. *

Size distribution information about the hydrometeors within the melting zone is not provided in this report but will be furnished later. The hydrometeors in this zone are composed of fully-melted water drops and water-coated ice particles in varying proportions, dependent on the temperature structure of the atmosphere and the altitude within the zone. Spectrum assessments for both types of hydrometeors will be presented as functions of altitude, decreasing downward from the upper boundary of the melting zone to the lower boundary.

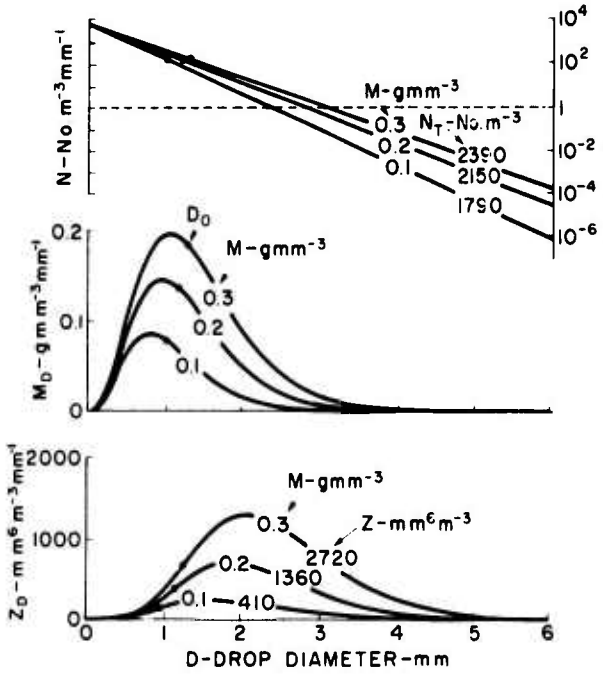

Figure 13. Distribution-Function Plots for Rain, Type R_{JW}, for Three Different Values of Liquid-Water-Content. The plots are similar to those for ice-crystals and snow, except that only one abscissa diameter scale is shown which extends to 6 mm

*Generally true for rain and large-snow, but exceptions can occur for appreciable lower diameter truncation in the case of small-snow and particularly in the case of ice crystals.

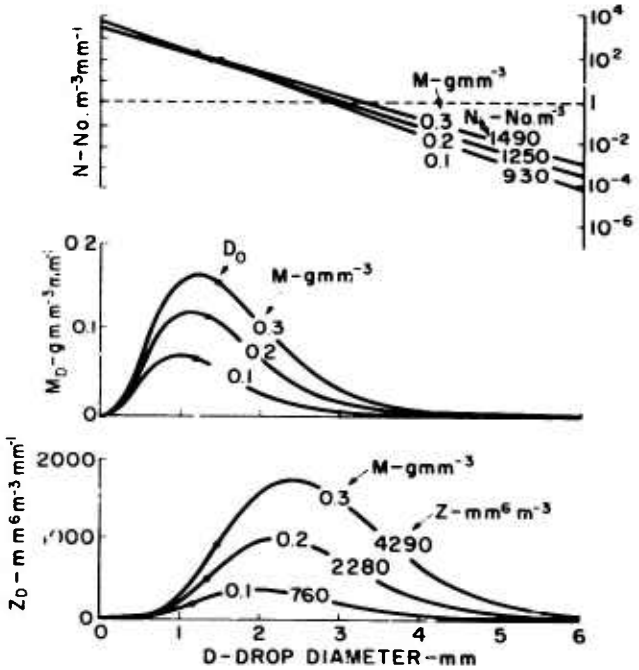

Figure 14. Distribution-Function Plots for Rain, of the Type Measured by the AFCRL Disdrometer Instruments on the SAMS Flight Day of 3 February 1972. Plots are shown for three values of liquid-water-content, 0.1, 0.2, nd 0.3 gm m^{-3}. The plots are otherwise similar to those of Figure 13

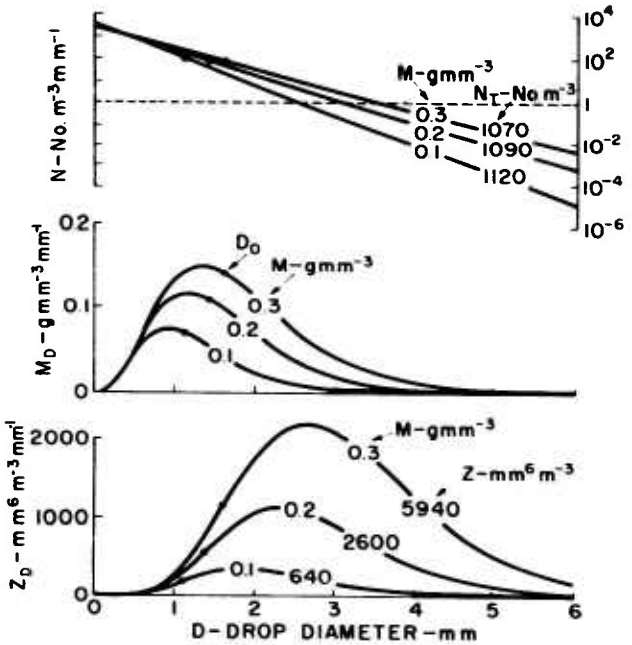

Figure 15. Distribution-Function Plots for Rain, of the Type Measured by the AFCRL Disdrometers on the SAMS Flight Day of 17 February 1972. (See the captions of Figures 9 and 14)

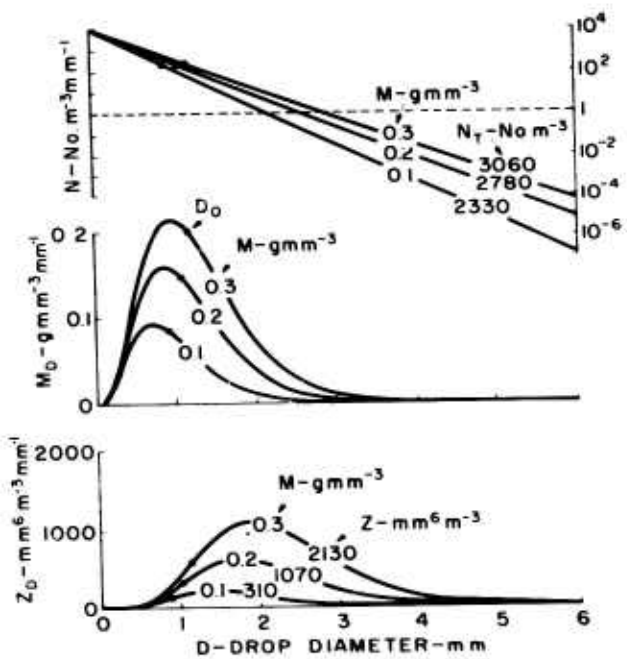

Figure 16. Distribution-Function Plots for Rain, of the Type Measured by the AFCRL Disdrometers on the SAMS Flight Day of 17 March 1972. (See the captions of Figures 9 and 14)

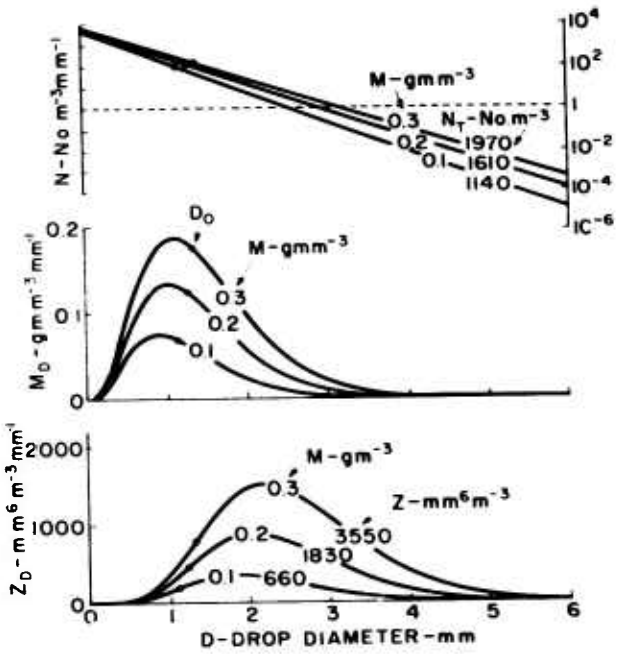

Figure 17. Distribution-Function Plots for Rain, of the Type Measured by the AFCRL Disdrometers on the SAMS Flight Day of 22 March 1972. (See the captions of Figures 9 and 14)

8. CONCLUDING REMARKS

This report has described how values of liquid-water-content in the precipitation size-range of the hydrometeors were determined for the SAMS missile trajectories from AFCRL-acquired radar and aircraft data. The accuracy of the liquid-water-content values were estimated to a first approximation, and information was supplied about the size spectra of the hydrometeors as assessed from theoretical distribution functions.

It should be emphasized that substantial liquid-water-content also exists in the cloud-size range of the hydrometeors, in which the droplets or particles are smaller than about 80 microns diameter (equivalent melted diameter, in the case of ice hydrometeors). The RARF radars at Wallops Island do not generally detect the presence of these cloud-size droplets or particles; consequently their numbers, sizes, and liquid-water-content must be determined from aircraft measurements. Aircraft data and size-distribution information concerning this "cloud-size portion" of the total hydrometeor spectrum will be included in later reports.

References

1. Plank, V.G. (1974) A summary of the radar equations and measurement techniques used in the SAMS rain erosion program at Wallops Island, Virginia, AFCRL/SAMS Report No. 1, 108 pps, AFCRL-TR-74-0053, Special Reports No. 172, Air Force Cambridge Research Laboratories, Bedford, Mass.
2. Wexler, R. (1947) Radar detection of a frontal storm, 18 June 1946, J. Meteorol. 4:38-44.
3. Marshall, J.S., Langille, R.C., and Palmer, W.McK. (1947) Measurement of rainfall by radar, J. Meteorol. 4(6):186-192.
4. Marshall, J.S., and Palmer, W.McK. (1948) The distribution of raindrops with size, J. Meteorol. 5:165-166.
5. Laws, J.O., and Parsons, D.A. (1943) The relation of raindrop size to intensity, Trans. Amer. Geophys. Union 24(Part II):452-460.
6. Sivaramakrishnan, M.V. (1961) Studies of raindrop size characteristics in different types of tropical rain using a simple raindrop recorder, Indian J. Met. Geophys. 12:189 (478-9, 602, 609, 613).
7. Atlas, D. (1964) Advances in radar meteorology, Adv. Geophys. 10:317 (399, 434, 441, 449, 478, 481).
8. Stout, G.E., and Mueller, E.A. (1968) Survey of relationships between rainfall rate and radar reflectivity in the measurement of precipitation, J. Appl. Meteorol. 7:465 (478-9).
9. Battan, L.J. (1973) Radar Observation of the Atmosphere, The University of Chicago Press, Chicago, Ill.
10. Marshall, J.S., and Gunn, K.L.S. (1952) Measurement of snow parameters by radar, J. Meteorol. 9:322.
11. Langille, R.C., and Thain, R.S. (1951) Some quantitative measurements of three centimeter radar echoes from falling snow, Canadian J. Phys. 29:482.
12. Imai, I., Fujiwara, M., Ichimura, I., and Toyama, Y. (1955) Radar reflectivity of falling snow, Pap. in Meteorol. and Geophys. (Japan) 6:130-139.

References

13. Gunn, K. L. S., and Marshall, J. S. (1956) Size distributions of aggregate snowflakes, Scientific Report NW-20/B, USAF Contract AF19(122)-217, McGill Univ., Montreal, Canada.

14. Gunn, K. L. S., and Marshall, J. S. (1958) The distribution with size of aggregate snowflakes, J. Meteorol. 15:452(479).

15. Carlson, P. E., and Marshall, J. S. (1972) Measurement of snowfall by radar, J. Appl. Meteorol. 11:494-500.

16. Austin, P. M. (1963) Radar measurements of the distribution of precipitation in New England storms, Proc. 10th Weather Radar Conf., Washington, p. 247 (479, 481-482).

17. Ohtake, T., and Henmi, T. (1970) Radar Reflectivity of Aggregated Snowflakes, preprints of papers presented at the 14th Radar Meteorology Conf., Tucson, Arizona, 17-20 November 1970, pp. 209-211.

18. Langleben, M. P. (1954) The terminal velocity of snow aggregates, Quart. J. Meteorol. Soc. 80:174-181.

19. Kodaira, N., and Inaba, M. (1955) Measurement of snowfall intensity by radar, Papers Meteorol. Geophys. (Japan) 6:126-129.

20. Litvinov, I. V. (1956) Determination of the terminal velocity of snowflakes (in Russian), IZV. Akad. Nauk SSSR Ser. Geofiz. No. 7, p. 853 (242).

21. Bashkirova, G., and Pershina, T. (1964) On the mass of snow crystals and their fall velocities, Tr. Gl. Geofiz. Observ. No. 165, 83-100.

22. Kikuchi, K. (1968) On snow crystals of bullet type, J. Meteorol. Soc. Japan 46: 128-132.

23. Sekhon, R. S., and Srivastava, R. C. (1970) Snow size spectra and radar reflectivity, J. Atmos. Sci. 27:299-307.

24. Knollenberg, R. G. (1970) The optical array: An alternative to scattering or extinction for airborne particle size determination, J. Appl. Meteor. 9:86-103.

25. Knollenberg, R. G. (1972) Measurements of the growth of the ice budget in a persisting contrail, J. Atmos. Sci. 29:1367-1374.

26. Knollenberg, R. G. (1973) Cirrus-contrail cloud spectra studies with the Sabreliner, Atmos. Tech., National Center for Atmospheric Research, No. 1, March 1973, pps. 52-55.

27. Heymsfield, A. J., and Knollenberg, R. G. (1972) Properties of cirrus-generating cells, J. Atmos. Sci. 29(7), 1358-1366.

28. Boucher, R. J., and Bartnoff, S. (1955) A Comparison of Theoretically Derived and Observed Drop-Size Distributions in Clouds and Rain, Tufts University, Dept. of Physics, Sci. Rept No. 4 under Contract AF 19(604)-550, 30 pp.

29. Joss, J., Schram, Karin, Thams, J. C., and Waldvogel, A. (1970) On the Quantitative Determination of Precipitation by Radar, Wissenschaftliche Mitteilung Nr. 63 Forschungsstelle der "Eidgenossischen Kommission zum Studium der Hagelbildung und der Hagelabwehr" am Osservatorio Ticinese della Centrale Meteorologica Svizzera, Locarno-Monti.

30. Sekhon, R. S., and Srivastava, R. C. (1971) Doppler radar observations of drop size distributions in a thunderstorm, J. Atmos. Sci. 28:983-994.

31. Spilhaus, A. F. (1948) Raindrop size, shape, and falling speed, J. Meteorol. 5:108-110.

32. Gunn, R., and Kinzer, G. D. (1949) The terminal velocity of fall for water droplets in stagnant air, J. Meteorol. 6:243 (565, 594, 596-7).

33. Mason, B. J. (1971) The Physics of Clouds, Second Edition, Clarendon Press, Oxford, England.

34. Mueller, E. A., and Sims, A. L. (1966) The influence of sampling volume on raindrop size spectra, Proc. 12th Weather Radar Conf., Norman, Oklahoma, p. 135 (479, 608).

35. Hooper, J. E. N., and Kippax, A. A. (1950) Radar echoes from meteorological precipitation, Proc. I. E. E. 97(Pt. 1):89.

36. Hood, A. D. (1950) Quantitative measurements at 3 and 10 centimetres of radar intensities from precipitation, Nat. Res. Counc., Rpt No. 2155, Ottawa.

37. Austin, P. M., and Williams, E. L. (1951) Comparison of radar signal intensity with precipitation rate, M. I. T. Weather Radar Research, Tech. Rpt No. 14.

38. Doherty, L. H. (1963) The scattering coefficient of rain from forward scatter measurements, Proc. of the Tenth Weather Radar Conf., A. M. S., Boston, p. 171.

39. Austin, P. M. (1964) Radar measurements of precipitation rate, Proc. of the Eleventh Radar Conf.

40. Joss, J., Thams, J. C., and Waldvogel, A. (1968) The variation of raindrop size distributions at Locarno, Proc. Internatl. Conf. on Cloud Physics, Toronto, Amer. Meteorol. Soc., Boston, p. 369.

41. Weickmann, H. (1947) Die Eisphäse in der Atmosphäre, Library Trans. 273, Royal Aircraft Establishment, Farnborough, 96 pp.

42. Magono, C. (1953) On the growth of snowflakes and graupel., Scient. Rpt Yokohama Univ., Ser. 1, No. 2, p. 18 (239, 241, 242).

43. Borovikov, A. M. (1953) Some results on an investigation of the structure of crystal clouds (in Russian) Trudy Tsentral. Acrolog. Obs. No. 12 (247).

44. Hosler, C. L., Jensen, D. C., and Goldshlak, L. (1957) On the aggregation of ice crystals to form snow, J. Meteorol. 14:415 (250).

45. Hobbs, P. V. (1969) Ice multiplication in clouds, J. Atmos. Sci. 26:315-318.

46. Ono, A. (1970) Growth mode of ice crystals in natural clouds, J. Appl. Sci. 27(4):649-658.

47. Ludlam, F. H. (1947) The forms of ice clouds, Quart. J. Roy. Meteorol. Soc. 74:39-56.

48. Nakaya, J. (1951) The formation of ice crystals, Compendium of Meteorol., Boston, Amer. Meteorol. Soc. 207-220.

49. Gold, L. W., and Power, B. A. (1952) Correlation of snow-crystal type with estimated temperature of formation, J. Meteorol. 9:447 (246-7).

50. Gold, L. W., and Power, B. A. (1954) Dependence of the forms of natural snow crystals on meteorological conditions, J. Meteorol. 11:35 (247).

51. Hosler, C. L. (1954) Factors governing the temperature of ice-crystal formation in clouds, Proc. Toronto Met. Conf., 1953, p. 253, R. Met. Soc., London (157).

52. Magono, C., and Lee, C. W. (1966) Meteorological classification of natural snow crystals, J. Fac. Sci., Hokkaido Univ. 2(Ser. VII):321-335.

53. Magono, C. (1957) On snowflakes, Proc. Sixth Wea. Radar Conf., pp. 31-36, Boston, Am. Meteorol. Soc.

54. Marshall, J. S., and Langleben, M. P. (1954) A theory of snow-crystal habit and growth, J. Meteorol. 11:104 (254-6).

55. Nakaya, U., Hanajima, M., and Muguruma, J. (1958) Physical investigations on the growth of snow crystals, J. Fac. Sci., Hokkaido Univ., Ser. II, 5, 87 (265).

56. Hosler, C. L., and Hallgren, R. E. (1961) Ice crystal aggregation, Nubila 4: 13 (249).

57. Podzimek, J. (1968) Aerodynamic conditions of ice crystal aggregation, Proc. Internatl. Conf. Cloud Phys., Toronto, 295-299.

58. Huschke, R. E. (1959) Glossary of Meteorology, Amer. Meteorol. Soc., Boston, Mass.

59. Eshbach, O. W. (1957) Handbook of Engineering Fundamentals, John Wiley and Sons, Inc., New York, N. Y., Sixth Printing.

60. Atlas, D. (1953) Optical extinction by rainfall, J. Meteorol. 10:486-488.

Bibliography

Auer, A., and Veal, D. (1970) The dimensions of ice crystals in natural clouds, J. Atmos. Sci. 27:919-926.

Beard, K. V., and Pruppacher, H. R. (1969) A determination of the terminal velocity and drag of small water drops by means of a wind tunnel, J. Atmos. Sci. 26:1066 (593).

Bent, A. E. (1946) Radar detection of precipitation, J. Meteorol. 3:78-84.

Best, A. C. (1950) The size distribution of raindrops, Quart. J. Roy. Meteorol. Soc. 76:16-36.

Borovikov, A. M., Khrgian, A. Kh. et al (1961) Fizika Oblakov (Cloud Physics). Gidrometeor. Izdatel'stvo, Leningrad (English translation by Israel Program for Scientific Translations, Jerusalem, 1963), (110, 121, 382).

Boucher, R. J. (1951) Results of measurements of raindrop size, Proc. Conf. on Water Resources, pp. 293-97, Bull. 41, Aurbana, Illinois State Water Survey.

Brown, S. (1970) The terminal velocities of ice crystals, Preprints, Intern. Conf., Cloud Physics, Fort Collins, Colo., Am. Meteorol. Soc., 47-48.

Brown, E. N., and Braham, R. R., Jr. (1963) Precipitation particle measurements in cumulus congestus, J. Atmos. Sci. 20:23-28.

Cataneo, R. A. (1969) A method for estimating rainfall rate-radar reflectivity relationships, J. Appl. Meteorol. 8:315-19.

Cole, A. E., Donaldson, R. J., Dyer, R., Kantor, A. J., and Skrivanek, R. A. (1969) Precipitation and clouds: a revision of chapter 5, Handbook of Geophysics and Space Environments, Air Force Surveys in Geophys. No. 212, AFCRL-69-0487, Air Force Cambridge Research Laboratories, Bedford, Mass.

Cornford, S. (1965) Fall speeds of precipitation elements, Quart. J. Roy. Meteorol. Soc. 91:91-94.

Douglas, R. H., Gunn, K. L. S., and Marshall, J. S. (1957) Pattern in the vertical of snow generation, J. Meteorol. 14:95-114.

Foote, G. B., and du Toit, P. S. (1969) Terminal velocity of raindrops aloft, J. Appl. Meteorol. 8:249-53.

Fujiwara, M. (1965) Raindrop-size distributions from individual storms, J. Atmos. Sci. 22:585.

Hardy, K. R. (1967) Distributions and compositions of clouds at supersonic aircraft altitudes. II. Radar observations of cirrus clouds. Proc. Second Conf. Rain Erosion and Allied Phenomena, Meersburg, Germany.

Heymsfield, A. J. (1972) Ice crystal terminal velocities, J. Atmos. Sci. 29:1348-1357.

James, D. G. (1957) Investigations relating to cirrus clouds, Meteorol. Mag. 86:1.

Jayaweera, K. O. K. F., and Cottis, R. E. (1969) Fall velocities of platelike and columnar ice crystals, Quart. J. Roy. Meteorol. Soc. 95:703-709.

Jones, D. M. A. (1956) Rainfall drop size-distribution and radar reflectivity, Res. Rpt No. 6, Signal Corps Proj. 172B, Illinois State Water Survey, 20 pp.

Jones, R. F. (1960) Size-distribution of ice crystals in cumulo-nimbus clouds, Quart. J. Roy. Meteorol. Soc. 86:187-194.

Joss, J., and Waldvogel, A. (1969) Raindrop size distribution and sampling size errors, J. Atmos. Sci. 26:566.

Kessler, E. (1967) On the continuity of water substance, NSSL Tech. Memo No. 33, Environmental Science Services Administration, U. S. Dept. of Commerce.

Langille, R. C., and Thain, R. S. (1951) Some quantitative measurements of three centimeter radar echoes from falling snow, Canad. J. Phys. 29:482.

Langleben, M. P. (1954) The terminal velocity of snow aggregates, Quart. J. R. Meteorol. Soc. 80:174-181.

Laws, J. O. (1941) Measurements of the fall-velocity of water drops and raindrops, Trans. Aner. Geophys. Union 22:709-21.

Levin, L. M. (1954) Distribution function of cloud and raindrops by sizes, Dokl. Akad. Nauk SSSR 94:1045 (113).

Marshall, J. S. (1953) Precipitation trajectories and patterns, J. Meteorol. 10:25 (469-70).

Mason, B. J. (1955) Radar evidence for aggregation and orientation of melting snowflakes, Quart. J. R. Meteorol. Soc. 81:262-264.

Magono, C. (1954) On the falling velocity of solid precipitation elements, Sci. Rpt Yokohama Natl. Univ., Sec. II, I, No. 3, 33-40.

Magono, C. (1968) On the additional nucleation of natural snow crystals, J. Rech. Atmos. 3:147-152.

Mueller, E. A., and Jones, D. M. A. (1960) Drop size distributions in Florida, Proc. 8th Weather Radar Conf., Am. Meteorol. Soc., Boston, pp. 299-305.

Mueller, E. A., and Sims, A. L. (1966) Investigation of the quantitative determination of point and areal precipitation by radar echo measurements, Illinois State Water Survey Technical Report ECOM-00032-F, Contract DA-28-043 HMC-00032(E).

Nakaya, U. (1954) Snow Crystals, Harvard University Press, Cambridge, 510 pp.

Nakaya, U. (1955) Snow crystals and aerosols, J. Fac. Sci. Hokkaido Univ. 4:341 (264).

Nakaya, U., and Terada, T. (1935) Simultaneous observations of the mass, falling velocity and form of individual snow crystals, J. Fac. Sci. Hokkaido Univ., Ser. II, 1, 191-200.

Ono, A. (1969) The shape and riming properties of ice crystals in natural clouds, J. Atmos. Sci. 26:138-147.

Ramana Murty, Bh. V., and Gupta, S. C. (1959) Precipitation characteristics based on raindrop size measurements at Delhi and Khandala during southwest monsoon, J. Sci. Industr. Res. 18A:352.

Rigby, E. C., and Marshall, J. S. (1952) Modification of rain with distance fallen, McGill Univ. Stormy Weather Group, Sci. Rpt MW-3 (613).

Rigby, E. C., Marshall, J. S., and Hitschfeld, W. (1954) The development of the size distribution of raindrops during their fall, J. Meteorol. 11.363-372.

Spilhaus, A. F. (1948) Drop size intensity and radar echo of rain, J. Meteorol. 5: 161-64.

Stephens, J. J. (1962) Radar Characteristics of an Exponential Drop-Size Distribution With Application to a Dual-Frequency System, EERL Report under National Science Foundation Grant NSF G22115, 89 pp., Univ. of Texas, Austin.

Wexler, R. (1948) Rain intensities by radar, J. Meteorol. 5:171-173.

Wexler, R., and Atlas, D. (1958) Moisture supply and growth of stratiform precipitation, J. Meteorol. 15:531-538.

Yagi, T. (1970) Measurement of the fall velocity of ice crystals drifting in supercooled fog, J. Meteorol. Soc. Japan 48:287-292.

List of Symbols

Arabic Symbols

a	constant of the fall velocity equation for hydrometeors
A_s	horizontal sampling area of an instrument that measures rainfall or rainfall rate
b	exponent of the fall velocity equation for hydrometeors
d	vertical distance downward within the hydrometeor transition zones
D	diameter of water drops, also used in the general sense to include the equivalent melted diameter of ice hydrometeors
D_e	equivalent melted diameter of ice hydrometeors
D_i	drop diameter, for classified data
D_{e_i}	equivalent melted diameter, for classified data
D_o	median volume diameter (or median equivalent melted diameter) of the drops or ice particles of a given population
D'	modal diameter (or modal equivalent melted diameter) of the distribution of liquid-water-content; that is, the diameter (class) corresponding to the peak value of liquid-water-content
D'_Z	modal diameter (or modal equivalent melted diameter) of the distribution of the radar reflectivity factor; that is, the diameter (class) corresponding to the peak value of the radar reflectivity factor
dE_M	uncertainty of the values of the exponent of the M vs Z equation
dK_M	uncertainty of the values of the constant of the M vs Z equation
dM	uncertainty of the values of liquid-water-content (in the precipitation size range of the drops or particles)
dZ_{rm}	uncertainty of the radar-measured values of the radar reflectivity factor

dZ_s	uncertainty; that is, scatter, of the radar reflectivity values (used in regression analyses) about the regression line
e	base of natural logarithms
E	exponent of the Z vs P equation
E_M	exponent of the M vs Z equation
E_P	exponent of the P vs Z equation
h	vertical distance upward within the hydrometeor transition zones
H	vertical thickness of the hydrometeor transition zones
$\bar{I}$	radar integration signal, in absolute units of cm^{-1}
$\underline{\bar{I}}$	radar integration signal, decibel values
k	constant of the M vs P equation
$k_{subscript}$	constant of the M vs P equation for hydrometeor region and type, or other conditions, identified by the particular subscript
K	constant of the Z vs P equation
K_M	constant of the M vs Z equation
K_P	constant of the P vs Z equation
ℓ	approximate, average physical size of the ice hydrometeors; that is, of the snow aggregates or ice crystals
L	length
M	liquid-water-content, of precipitation-size hydrometeors
M_D	distributed liquid-water-content—distributed according to the diameter, or equivalent melted diameter, of the hydrometeor drops or particles—per millimeter bandwidth
$M_{subscript}$	liquid-water-content for the hydrometeor region and type, or other conditions, identified by the particular subscript
N	number concentration of the hydrometeor drops or particles per m^3 per mm bandwidth
N_o	constant of the non-truncated exponential-distribution-function specifying the variation of the number concentration of the drops or particles with the diameter, or equivalent melted diameter
N_T	total number of the hydrometeor drops or particles of a given population, per m^3
$N(D_i)$	number of drops of a classified diameter size, D_i, per cubic meter
$N(D_{e_i})$	number of snow or ice particles of a classified equivalent-melted-diameter, D_{e_i}, per cubic meter
$N_f(D_i)$	number of drops of a classified diameter size, D_i, that fall across a given horizontal area in a given time—dimensionless
$N_s(D_i)$	number of drops of a classified diameter size, D_i, that are included in a given volumetric sample—dimensionless
N[f(D)]	any general distribution function that specifies the number concentration of water drops as a function of their diameter

$N[f(D_e)]$	any general distribution function that specifies the number concentration of snow particles or ice crystals as a function of their equivalent melted diameter
P	precipitation rate, general
$P_{subscript}$	precipitation rate for the hydrometeor region and type, or other conditions, identified by the particular subscript
R_s	path distance along the SAMS missile trajectory
T	time
V	fall velocity of the drops or ice particles
V_{D_i}	fall velocity of a given size class of hydrometeors having the mid-diameter D_i
V_s	sampling volume
z	absolute altitude, above sea level
Δz	incremental difference of altitude
Z	radar reflectivity factor, general
Z_D	distributed radar reflectivity factor—distributed according to the diameter, or equivalent melted diameter, of the hydrometeor drops or particles—per millimeter bandwidth
Z_I	radar reflectivity factor for ice hydrometeors, as measured by radar
Z_{I_M}	radar reflectivity factor for ice hydrometeors, as computed from size-distribution data
Z_{I_T}	radar reflectivity factor for ice hydrometeors, as computed from the assumption of a theoretical distribution function
Z_W	radar reflectivity factor for water hydrometeors, as measured by radar
Z_{W_M}	radar reflectivity factor for water hydrometeors, as computed from size distribution data
Z_{W_T}	radar reflectivity factor for water hydrometeors, as computed from the assumption of a theoretical distribution function

Greek Symbols

α	constant of the exponential distribution function of Marshall and Palmer
$\alpha_{subscript}$	altitude change of the precipitation rate within the hydrometeor transition zone indicated by the particular subscript
$\beta_{subscript}$	altitude change of the constant of the M vs P equation within the hydrometeor transition zone indicated by the particular subscript
$\Gamma(n)$	gamma function of the particular number "n".
$\gamma_{subscript}$	altitude change of the exponent of the M vs P equation within the hydrometeor transition zone indicated by the particular subscript

ϵ	exponent of the M vs P equation
$\epsilon_{\text{subscript}}$	exponent of the M vs P equation for the hydrometeor region and type, or other conditions, identified by the particular subscript
η	radar volume reflectivity, in absolute units of cm^{-1}
$\underline{\eta}$	radar volume reflectivity, decibel values
λ	radar wavelength
Λ	exponential "slope factor" in the distribution function for the number concentration of the drops or particles
π	circle circumference divided by diameter
ρ_w	density of water
ϕ	elevation angle of the SAMS missile trajectory above the horizontal plane
$\sigma_{\overline{P}_{r_1}}$	standard deviation of pulse or video integrated received power for single independent samples

Other Symbols

$\underline{\ }$	when used to "underline" any given Arabic or Greek symbol, represents the decibel equivalent value of the parameter; for example, $\underline{X} = 10 \log X$.

☆ U. S. GOVERNMENT PRINTING OFFICE: 1974--600-013--10